Drug treatment and viable cell count

Either DMSO or 10 μM Rosco was diluted in media and added to cells every 3 days for 30 days when the cells were passaged. At the same time, the number of cells was determined by counting the viable cells with a hemocytometer using the Trypan blue dye exclusion assay. For each period, three dishes of each group were counted. At 23 d.p.i., cells were stained with 2 μg/ml of propidium iodide (PI) in growth media, then CPE- and PI-positive cells were evaluated under an inverted fluorescence/phase-contrast microscopy (Olympus, Tokyo, Japan).

Hemagglutination (HA) assay

JCV titers were assayed by hemagglutination of human type O erythrocytes as described previously (Suzuki et al., 2001). JCI cells were collected after treatment with 0 μM (DMSO only), 5 μM, or 10 μM of Roscovitine for 12 days. The media, with or without Roscovitine, were changed every 3 days. The cells (1×10^6) were washed in phosphate-buffered saline (PBS), resuspended with 50 μl of Tris-HCl (pH 7.5) containing 0.2% BSA, and treated with 0.05 U/ml of neuraminidase as described above. For the hemagglutination assay, two-fold serial dilutions of the cell extract (25 μl) with PBS (pH 7.15) containing 0.2% BSA were made in 96-well, V-bottomed microplates. An equal volume of 0.5% red blood cells in PBS (pH 7.15) was added to each well. Cells were incubated at 4 °C for 3 h, at which point the HA titer of virus was expressed as the highest dilution resulting in hemagglutination.

Immunocytochemistry

JCV-infected IMR-32 cells were fixed for 3 min in 100% methanol at −20 °C. After blocking with 1% BSA, cells were incubated with anti-VP1 antibody (1:5,000) overnight at 4 °C, and stained with Alexa Fluor 488-conjugated anti-rabbit immunoglobulin antibody (1:500; Invitrogen, Carlsbad, CA) for 1 h at room temperature. Cells positive for VP1 were observed under an inverted fluorescence/phase-contrast microscopy (Olympus).

Immunoblotting and immunoprecipitation

Either IMR-32 cells inoculated with 800 HA units of the JCV in 4 ml of growth media or JCI cells were collected at various days in the presence or absence of Rosco and lysed in lysis buffer [1% Triton X-100, 150 mM NaCl, 0.1% sodium dodecyl sulfate (SDS), 1% deoxycholic acid, 10 mM Tris-HCl (pH 7.5), 5 mM EDTA, 10% glycerol, 50 mM sodium fluoride, and 1 mM phenylmethylsulfonyl fluoride]. After sonication and centrifugation, 10 μg of protein was separated by SDS–PAGE and examined by immunoblotting using anti-VP1 (1:5,000), anti-agnoprotein (1:3,000), anti-SV40 large T (1:500), and anti-α-tubulin (1:5,000) antibodies. After incubation with horseradish peroxidase-conjugated secondary antibody (1:3,000; Biosource International, Camarillo, CA), the signal was detected with an ECL detection kit (GE Healthcare Bio-Sciences, Piscataway, NJ) and visualized with a LAS-1000 plus system (Fujifilm, Tokyo, Japan).

For immunoprecipitation, cells were lysed in IP lysis buffer [1% NP40, 150 mM NaCl, 10 mM Tris-HCl (pH 7.5), 1 mM EDTA, 50 mM sodium fluoride, 1 mM phenylmethylsulfonyl fluoride, 1 mM sodium orthovanadate, complete protease inhibitor cocktail (Roche, Basel, Switzerland), and phosphatase inhibitor cocktail 1 (Sigma)]. Lysed protein was pre-incubated with 20 μl of protein G Sepharose (GE Healthcare Bio-Sciences) at 4 °C for 1 h. The supernatant was incubated with anti-large T antibody or normal mouse IgG at 4 °C for 3 h. Protein complexes were pulled down by incubation with protein G Sepharose at 4 °C for 2 h and elution with SDS sample buffer [125 mM Tris-HCl (pH 6.8), 10% 2-mercaptoethanol, 4% SDS, 10% sucrose, and 0.04% bromophenol blue] after washing with IP lysis buffer. Immunoblotting was carried out with the anti-phospho-Thr-Pro antibody (1:5,000) and horseradish peroxidase-conjugated anti-mouse IgM (1:3,000; Zymed, South San Francisco, CA) secondary antibody. Signals were analyzed as described above.

Flow cytometry

For flow cytometry analysis of TAg expression, JCI cells were collected, washed twice with PBS, suspended, and fixed with 70% ice-cold ethanol overnight at 4 °C. Cells were washed with PBS containing 0.5% fetal bovine albumin, incubated with anti-SV40 TAg (Ab-2) antibody at room temperature for 2 h and stained with fluorescein isothiocyanate (FITC)-conjugated anti-mouse IgG (Beckman Coulter, Fullerton, CA) at room temperature for 1 h. Flow cytometry experiments were carried out using a FACSCalibur system (BD Biosciences, Sun Jose, CA) and data were analyzed using Flowjo software (Tree Star, Ashland, OR).

Reverse transcription (RT) and real-time PCR

For RNA extraction, JCI cells were collected after varying durations of treatment with DMSO or 10 μM Roscovitine. Total RNA was isolated using an RNeasy Mini Kit (Qiagen, Valencia, CA) according to the manufacturer's protocol. Total RNA (1 μg) was treated with DNase I (Invitrogen) at 37 °C for 1 h in 10 μl of reaction mixture. After inactivation of DNase I with 2.5 mM EDTA at 65 °C for 15 min, 4 μl of reaction mixture was used for RT using a Superscript first-strand synthesis system (Invitrogen). To confirm that the samples were not contaminated with genomic DNA, RNase-free water was added instead of Superscript II reverse transcriptase to at least one negative control sample that was run in parallel. After confirmation of cDNA amplification by conventional PCR for β-actin and VP1, real-time PCR was performed using 0.5 μl of reaction mixture containing cDNA, SYBR green PCR Master Mix (Applied Biosystems, Foster City, CA), and gene-specific primer sets: JCV large T, 5′-AAA GTT GCT CAT CAG CCT GAT TTT-3′ and 5′-CAT CCC ACT TCT CAT TAA ATG TAT TCC-3′; JCV agnoprotein, 5′-CCA GCT GTC ACG TAA GGC TTC T-3′ and 5′-GTG CAA AAG TCC AGC AAA AAT TC-3′; JCV VP1, 5′-

TCT AAA TGA GGA TCT AAC CTG TGG AAA-3′ and 5′-GCC CAT TAG AGT GCA CAT TCA TC-3′; β-actin, 5′-TTG CCG ACA GGA TGC AGA A-3′ and 5′-GCC GAT CCA CAC GGA GTA CT-3′. After incubation of mixtures at 50 °C for 2 min and 95 °C for 10 min, the reaction was performed at 95 °C for 15 s and 60 °C for 1 min for 40 cycles using a GeneAmp 5700 Sequence Detection System (Applied Biosystems). The levels of PCR products were analyzed with GeneAmp 5700 SDS software (Applied Biosystems) and cycle times were normalized to the cycle time of β-actin (Orba et al., 2004). All reactions were confirmed by at least three independent experiments.

Luciferase assay and JCV transcription assay

Firefly luciferase reporter vectors pGL3-Basic and the internal *Renilla* luciferase control vector phRL-TK were purchased from Promega (Madison, WI). JCV early and late reporter vectors (pGL3-Early or pGL3-Late) were constructed from the regulatory regions of JCV Mad1 that has been previously described (Okada et al., 2000). For the luciferase assay, IMR-32 cells were seeded onto 24-well plates and the cells were treated with DMSO or 10 μM Roscovitine for 48 h. Each pGL3 reporter vector and phRL-TK control vector were co-transfected into the cells using Lipofectamine 2000 (Invitrogen) according to the manufacturer's instructions. Six hours after transfection, the media on each plate of cells were replaced with fresh media containing DMSO or Roscovitine and the cells were cultured for another 48 h. Luciferase activity of the cells was measured using a dual-luciferase reporter assay system (Promega) according to the manufacturer's instructions. Luminescence intensity was measured with a Luminometer (Turner Designs, Sunnyvale, CA). The firefly luciferase activity data are presented as mean values ± SD. The results of each experiment were confirmed by three independent transfections. We could not use *Renilla* luciferase activity for normalization of the firefly luciferase activity because Roscovitine seems to affect *Renilla* luciferase activity derived from phRL-TK with the HSV-TK promoter (Schang et al., 1999). The pJCE and pJCL reporter plasmids for the analysis of JCV transcriptional activity were constructed as follows: the early (E) and late (L) genes of the JCV Mad1 strain containing the TCR and poly-adenylation signal were amplified by PCR and subcloned into pGL3-basic that had been digested with *Nhe*I and *Sal*I. IMR-32 cells were seeded onto 6-well plates and transfected with pGL3 basic, pJCE, or pJCL. Six hours after transfection, the media on each plate of cells were replaced with fresh media containing DMSO or Roscovitine and the cells were cultured for 48 h. RNA extraction and reverse transcription were performed as described above. To detect pJCE- or pJCL-specific transcripts, PCR analyses of the synthesized cDNA were carried out using Taq DNA polymerase (Sigma). For detection of early transcripts, the primer pairs of JCV large T: 5′-AAA GTT GCT CAT CAG CCT GAT TTT-3′ and 5′-CAT CCC ACT TCT CAT TAA ATG TAT TCC-3′, and for late transcripts, the primer pairs of JCV VP1: 5′-AAT GTG CAC TCT AAT GGG CAA GC-3′ and 5′-CTA GGT ACG CCT TGT GCT CTG-3′ were used. As a control, the primer pairs of glyceraldehyde 3-phosphate dehydrogenase (GAPDH): 5′-TTC GTC ATG GGT GTG AAC CA-3′ and 5′-GGT CAT GAG TCC TTC CAC GAT AC-3′ were used.

DpnI replication assay

The full-length of the JCV Mad1 transcriptional control region (TCR) was subcloned into a pBluescript II SK (+) vector, which was designated pBS-JCori. The JCV TAg expression vector $pCXN_2$-JCTAg was constructed from pBR-Mad1. IMR-32 cells were seeded onto 6 cm dishes and co-transfected with pBS-JCori and $pCXN_2$-JCTAg or a $pCXN_2$ empty vector using Lipofectamine 2000 according to the manufacturer's instructions. Six hours after transfection, the media on each plate of cells were replaced with fresh media containing DMSO or 10 μM Roscovitine and cells were cultured for 48 h. Low-molecular weight DNA was isolated from the cells according to the method of Hirt (1967). Extracts were treated with 0.5 mg/ml Proteinase K at 56 °C for 1 h prior to phenol/chloroform/isoamyl alcohol and ethanol precipitation. DNA was suspended in TE [10 mM Tris-HCl (pH 7.5), 1 mM EDTA (pH 8.0)] containing 75 μg/ml RNase A. Sample DNA (5 μg) was digested with *Eco*RI and *Dpn*I, which selectively digest transfected DNA that has been methylated during prokaryotic replication, and digested products were separated by electrophoresis on a 1% agarose gel. DNA fragments were transferred to a Hybond N^+ membrane (GE Healthcare Bio-Sciences) by capillary transfer using 20× SSC transfer buffer. The immobilized DNA was detected using a digoxigenin-labeled DNA probe that encoded a vector-derived ampicillin-resistant DNA sequence (DIG high prime DNA labeling and detection starter kit II, Roche). Signals were visualized with the LAS-1000 plus system and replication activities were determined by quantifying the intensity of the bands using Multi Gauge software (Fujifilm). These results were confirmed by three independent experiments.

BrdU incorporation

For detection of BrdU incorporation by flow cytometry, 10 μM of BrdU (Sigma) was incorporated into the cells for 1 h after treatment with DMSO or 10 μM Roscovitine for 2 days. Cells were washed twice with PBS and suspended and fixed with 70% ice-cold ethanol overnight. DNA was denatured with 2 N HCl in PBS containing 0.1% Triton-X at room temperature for 20 min and neutralized with 0.1 M Sodium tetraborate (pH 9.0) for 5 min. Treated cells were washed in PBS containing 0.5% BSA, stained with Rat anti-BrdU antibody (1:50), and stained with FITC-conjugated anti-Rat IgG antibody. BrdU-positive cells were analyzed by flow cytometry as described above.

Statistics

Statistical comparisons between experimental groups were analyzed using the Student's *t*-test, and for all comparisons $p<0.05$ was considered significant.

Acknowledgments

This study was supported in part by grants from the Ministry of Education, Science, Sports, and Culture and by grants from the Ministry of Health, Labor and Welfare, Japan; the Japan Health Science Foundation; and the Program of Founding Research Centers for Emerging and Reemerging Infectious Diseases, MEXT Japan.

References

Agbottah, E., de La Fuente, C., Nekhai, S., Barnett, A., Gianella-Borradori, A., Pumfery, A., Kashanchi, F., 2005. Antiviral activity of CYC202 in HIV-1-infected cells. J. Biol. Chem. 280 (4), 3029–3042.

Albrecht, H., Hoffmann, C., Degen, O., Stoehr, A., Plettenberg, A., Mertenskotter, T., Eggers, C., Stellbrink, H.J., 1998. Highly active antiretroviral therapy significantly improves the prognosis of patients with HIV-associated progressive multifocal leukoencephalopathy. Aids 12 (10), 1149–1154.

Amemiya, K., Traub, R., Durham, L., Major, E.O., 1989. Interaction of a nuclear factor-1-like protein with the regulatory region of the human *Polyomavirus* JC virus. J. Biol. Chem. 264 (12), 7025–7032.

Ariza, A., Mate, J.L., Isamat, M., Calatrava, A., Fernandez-Vasalo, A., Navas-Palacios, J.J., 1998. Overexpression of Ki-67 and cyclins A and B1 in JC virus-infected cells of progressive multifocal leukoencephalopathy. J. Neuropathol. Exp. Neurol. 57 (3), 226–230.

Benson, C., White, J., De Bono, J., O'Donnell, A., Raynaud, F., Cruickshank, C., McGrath, H., Walton, M., Workman, P., Kaye, S., Cassidy, J., Gianella-Borradori, A., Judson, I., Twelves, C., 2007. A phase I trial of the selective oral cyclin-dependent kinase inhibitor seliciclib (CYC202; R-Roscovitine), administered twice daily for 7 days every 21 days. Br. J. Cancer 96 (1), 29–37.

Bresnahan, W.A., Boldogh, I., Chi, P., Thompson, E.A., Albrecht, T., 1997. Inhibition of cellular Cdk2 activity blocks human cytomegalovirus replication. Virology 231 (2), 239–247.

Canduri, F., Uchoa, H.B., de Azevedo Jr., W.F., 2004. Molecular models of cyclin-dependent kinase 1 complexed with inhibitors. Biochem. Biophys. Res. Commun. 324 (2), 661–666.

Collazos, J., Mayo, J., Martinez, E., Blanco, M.S., 1999. Contrast-enhancing progressive multifocal leukoencephalopathy as an immune reconstitution event in AIDS patients. Aids 13 (11), 1426–1428.

Davido, D.J., Leib, D.A., Schaffer, P.A., 2002. The cyclin-dependent kinase inhibitor roscovitine inhibits the transactivating activity and alters the posttranslational modification of herpes simplex virus type 1 ICP0. J. Virol. 76 (3), 1077–1088.

De Azevedo, W.F., Leclerc, S., Meijer, L., Havlicek, L., Strnad, M., Kim, S.H., 1997. Inhibition of cyclin-dependent kinases by purine analogues: crystal structure of human cdk2 complexed with roscovitine. Eur. J. Biochem. 243 (1–2), 518–526.

Elphick, G.F., Querbes, W., Jordan, J.A., Gee, G.V., Eash, S., Manley, K., Dugan, A., Stanifer, M., Bhatnagar, A., Kroeze, W.K., Roth, B.L., Atwood, W.J., 2004. The human *Polyomavirus*, JCV, uses serotonin receptors to infect cells. Science 306 (5700), 1380–1383.

Endo, S., Okada, Y., Orba, Y., Nishihara, H., Tanaka, S., Nagashima, K., Sawa, H., 2003. JC virus agnoprotein colocalizes with tubulin. J. Neurovirology 9 (Suppl 1), 10–14.

Habran, L., Bontems, S., Di Valentin, E., Sadzot-Delvaux, C., Piette, J., 2005. Varicella-zoster virus IE63 protein phosphorylation by roscovitine-sensitive cyclin-dependent kinases modulates its cellular localization and activity. J. Biol. Chem. 280 (32), 29135–29143.

Hall, C.D., Dafni, U., Simpson, D., Clifford, D., Wetherill, P.E., Cohen, B., McArthur, J., Hollander, H., Yainnoutsos, C., Major, E., Millar, L., Timpone, J., 1998. Failure of cytarabine in progressive multifocal leukoencephalopathy associated with human immunodeficiency virus infection. AIDS Clinical Trials Group 243 Team. N. Engl. J. Med. 338 (19), 1345–1351.

Hirt, B., 1967. Selective extraction of polyoma DNA from infected mouse cell cultures. J. Mol. Biol. 26 (2), 365–369.

Kerr, D., Chang, C.F., Chen, N., Gallia, G., Raj, G., Schwartz, B., Khalili, K., 1994. Transcription of a human neurotropic virus promoter in glial cells: effect of YB-1 on expression of the JC virus late gene. J. Virol. 68 (11), 7637–7643.

Kim, R.J., Moine, S., Reese, D.K., Bullock, P.A., 2002. Peptides containing cyclin/Cdk-nuclear localization signal motifs derived from viral initiator proteins bind to DNA when unphosphorylated. J. Virol. 76 (23), 11785–11792.

Komagome, R., Sawa, H., Suzuki, T., Suzuki, Y., Tanaka, S., Atwood, W.J., Nagashima, K., 2002. Oligosaccharides as receptors for JC virus. J. Virol. 76 (24), 12992–13000.

Kudoh, A., Daikoku, T., Sugaya, Y., Isomura, H., Fujita, M., Kiyono, T., Nishiyama, Y., Tsurumi, T., 2004. Inhibition of S-phase cyclin-dependent kinase activity blocks expression of Epstein–Barr virus immediate-early and early genes, preventing viral lytic replication. J. Virol. 78 (1), 104–115.

Marra, C.M., Rajicic, N., Barker, D.E., Cohen, B.A., Clifford, D., Donovan Post, M.J., Ruiz, A., Bowen, B.C., Huang, M.L., Queen-Baker, J., Andersen, J., Kelly, S., Shriver, S., 2002. A pilot study of cidofovir for progressive multifocal leukoencephalopathy in AIDS. Aids 16 (13), 1791–1797.

McClue, S.J., Blake, D., Clarke, R., Cowan, A., Cummings, L., Fischer, P.M., MacKenzie, M., Melville, J., Stewart, K., Wang, S., Zhelev, N., Zheleva, D., Lane, D.P., 2002. In vitro and in vivo antitumor properties of the cyclin dependent kinase inhibitor CYC202 (R-roscovitine). Int. J. Cancer 102 (5), 463–468.

McVey, D., Brizuela, L., Mohr, I., Marshak, D.R., Gluzman, Y., Beach, D., 1989. Phosphorylation of large tumour antigen by cdc2 stimulates SV40 DNA replication. Nature 341 (6242), 503–507.

McVey, D., Ray, S., Gluzman, Y., Berger, L., Wildeman, A.G., Marshak, D.R., Tegtmeyer, P., 1993. cdc2 phosphorylation of threonine 124 activates the origin-unwinding functions of simian virus 40 T antigen. J. Virol. 67, 5206–5215.

McVey, D., Woelker, B., Tegtmeyer, P., 1996. Mechanisms of simian virus 40 T-antigen activation by phosphorylation of threonine 124. J. Virol. 70 (6), 3887–3893.

Meijer, L., Borgne, A., Mulner, O., Chong, J.P., Blow, J.J., Inagaki, N., Inagaki, M., Delcros, J.G., Moulinoux, J.P., 1997. Biochemical and cellular effects of roscovitine, a potent and selective inhibitor of the cyclin-dependent kinases cdc2, cdk2 and cdk5. Eur. J. Biochem. 243 (1–2), 527–536.

Moarefi, I.F., Small, D., Gilbert, I., Hopfner, M., Randall, S.K., Schneider, C., Russo, A., Ramsperger, U., Arthur, A.K., Stahl, H., et al., 1993. Mutation of the cyclin-dependent kinase phosphorylation site in simian virus 40 (SV40) large T antigen specifically blocks SV40 origin DNA unwinding. J. Virol. 67 (8), 4992–5002.

Nukuzuma, S., Yogo, Y., Guo, J., Nukuzuma, C., Itoh, S., Shinohara, T., Nagashima, K., 1995. Establishment and characterization of a carrier cell culture producing high titres of polyoma JC virus. J. Med. Virol. 47 (4), 370–377.

Okada, Y., Sawa, H., Tanaka, S., Takada, A., Suzuki, S., Hasegawa, H., Umemura, T., Fujisawa, J., Tanaka, Y., Hall, W.W., Nagashima, K., 2000. Transcriptional activation of JC virus by human T-lymphotropic virus type I Tax protein in human neuronal cell lines. J. Biol. Chem. 275 (22), 17016–17023.

Okada, Y., Sawa, H., Endo, S., Orba, Y., Umemura, T., Nishihara, H., Stan, A.C., Tanaka, S., Takahashi, H., Nagashima, K., 2002. Expression of JC virus agnoprotein in progressive multifocal leukoencephalopathy brain. Acta Neuropathol. (Berl.) 104 (2), 130–136.

Orba, Y., Sawa, H., Iwata, H., Tanaka, S., Nagashima, K., 2004. Inhibition of virus production in JC virus-infected cells by postinfection RNA interference. J. Virol. 78 (13), 7270–7273.

Radhakrishnan, S., Gordon, J., Del Valle, L., Cui, J., Khalili, K., 2004. Intracellular approach for blocking JC virus gene expression by using RNA interference during viral infection. J. Virol. 78 (13), 7264–7269.

Ranganathan, P.N., Khalili, K., 1993. The transcriptional enhancer element, kappa B, regulates promoter activity of the human neurotropic virus, JCV, in cells derived from the CNS. Nucleic Acids Res. 21 (8), 1959–1964.

Raynaud, F.I., Whittaker, S.R., Fischer, P.M., McClue, S., Walton, M.I., Barrie,

S.E., Garrett, M.D., Rogers, P., Clarke, S.J., Kelland, L.R., Valenti, M., Brunton, L., Eccles, S., Lane, D.P., Workman, P., 2005. In vitro and in vivo pharmacokinetic-pharmacodynamic relationships for the trisubstituted aminopurine cyclin-dependent kinase inhibitors olomoucine, bohemine and CYC202. Clin. Cancer Res. 11 (13), 4875–4887.

Ruffini, F., Arbour, N., Blain, M., Olivier, A., Antel, J.P., 2004. Distinctive properties of human adult brain-derived myelin progenitor cells. Am. J. Pathol. 165 (6), 2167–2175.

Sadowska, B., Barrucco, R., Khalili, K., Safak, M., 2003. Regulation of human *Polyomavirus* JC virus gene transcription by AP-1 in glial cells. J. Virol. 77 (1), 665–672.

Sanchez, V., Spector, D.H., 2006. Cyclin-dependent kinase activity is required for efficient expression and posttranslational modification of human cytomegalovirus proteins and for production of extracellular particles. J. Virol. 80 (12), 5886–5896.

Sanchez, V., McElroy, A.K., Yen, J., Tamrakar, S., Clark, C.L., Schwartz, R.A., Spector, D.H., 2004. Cyclin-dependent kinase activity is required at early times for accurate processing and accumulation of the human cytomegalovirus UL122-123 and UL37 immediate-early transcripts and at later times for virus production. J. Virol. 78 (20), 11219–11232.

Schang, L.M., 2002. Cyclin-dependent kinases as cellular targets for antiviral drugs. J. Antimicrob. Chemother. 50 (6), 779–792.

Schang, L.M., 2004. Effects of pharmacological cyclin-dependent kinase inhibitors on viral transcription and replication. Biochim. Biophys. Acta 1697 (1–2), 197–209.

Schang, L.M., Phillips, J., Schaffer, P.A., 1998. Requirement for cellular cyclin-dependent kinases in herpes simplex virus replication and transcription. J. Virol. 72 (7), 5626–5637.

Schang, L.M., Rosenberg, A., Schaffer, P.A., 1999. Transcription of herpes simplex virus immediate-early and early genes is inhibited by roscovitine, an inhibitor specific for cellular cyclin-dependent kinases. J. Virol. 73 (3), 2161–2172.

Schang, L.M., Bantly, A., Knockaert, M., Shaheen, F., Meijer, L., Malim, M.H., Gray, N.S., Schaffer, P.A., 2002. Pharmacological cyclin-dependent kinase inhibitors inhibit replication of wild-type and drug-resistant strains of herpes simplex virus and human immunodeficiency virus type 1 by targeting cellular, not viral, proteins. J. Virol. 76 (15), 7874–7882.

Suzuki, S., Sawa, H., Komagome, R., Orba, Y., Yamada, M., Okada, Y., Ishida, Y., Nishihara, H., Tanaka, S., Nagashima, K., 2001. Broad distribution of the JC virus receptor contrasts with a marked cellular restriction of virus replication. Virology 286 (1), 100–112.

Swenson, J.J., Frisque, R.J., 1995. Biochemical characterization and localization of JC virus large T antigen phosphorylation domains. Virology 212 (2), 295–308.

Swenson, J.J., Trowbridge, P.W., Frisque, R.J., 1996. Replication activity of JC virus large T antigen phosphorylation and zinc finger domain mutants. J. Neurovirology 2 (2), 78–86.

Taylor, S.L., Kinchington, P.R., Brooks, A., Moffat, J.F., 2004. Roscovitine, a cyclin-dependent kinase inhibitor, prevents replication of varicella-zoster virus. J. Virol. 78 (6), 2853–2862.

Vita, M., Abdel-Rehim, M., Olofsson, S., Hassan, Z., Meurling, L., Siden, A., Siden, M., Pettersson, T., Hassan, M., 2005. Tissue distribution, pharmacokinetics and identification of roscovitine metabolites in rat. Eur. J. Pharm. Sci. 25 (1), 91–103.

Wang, D., de la Fuente, C., Deng, L., Wang, L., Zilberman, I., Eadie, C., Healey, M., Stein, D., Denny, T., Harrison, L.E., Meijer, L., Kashanchi, F., 2001. Inhibition of human immunodeficiency virus type 1 transcription by chemical cyclin-dependent kinase inhibitors. J. Virol. 75 (16), 7266–7279.

Wegner, M., Drolet, D.W., Rosenfeld, M.G., 1993. Regulation of JC virus by the POU-domain transcription factor Tst-1: implications for progressive multifocal leukoencephalopathy. Proc. Natl. Acad. Sci. U. S. A. 90 (10), 4743–4747.

Wroblewska, Z., Wellish, M., Gilden, D., 1980. Growth of JC virus in adult human brain cell cultures. Arch. Virol. 65 (2), 141–148.

Transgenic expression of *Helicobacter pylori* CagA induces gastrointestinal and hematopoietic neoplasms in mouse

Naomi Ohnishi*, Hitomi Yuasa*, Shinya Tanaka†, Hirofumi Sawa‡, Motohiro Miura*, Atsushi Matsui*, Hideaki Higashi*, Manabu Musashi§, Kazuya Iwabuchi¶, Misao Suzuki‖, Gen Yamada‖, Takeshi Azuma**, and Masanori Hatakeyama*††

*Division of Molecular Oncology, Institute for Genetic Medicine and Division of Chemistry, Graduate School of Science, §Health Administration Center, and ¶Division of Immunobiology, Institute for Genetic Medicine, Hokkaido University, Sapporo 060-0815, Japan; †Laboratory of Molecular and Cellular Pathology, Hokkaido University Graduate School of Medicine, Sapporo 060-8638, Japan; ‡Department of Molecular Pathobiology, Hokkaido University Research Center for Zoonosis Control, Sapporo 001-0020, Japan; ‖Center for Animal Resources and Development, Graduate School of Medical and Pharmaceutical Sciences, Kumamoto University, Kumamoto 860-0811, Japan; and **Department of Gastroenterology, Kobe University Graduate School of Medicine, Kobe 650-0017, Japan

Communicated by Tadatsugu Taniguchi, University of Tokyo, Tokyo, Japan, November 27, 2007 (received for review October 26, 2007)

Infection with *cagA*-positive *Helicobacter pylori* is associated with gastric adenocarcinoma and gastric mucosa-associated lymphoid tissue (MALT) lymphoma of B cell origin. The *cagA*-encoded CagA protein is delivered into gastric epithelial cells via the bacterial type IV secretion system and, upon tyrosine phosphorylation by Src family kinases, specifically binds to and aberrantly activates SHP-2 tyrosine phosphatase, a bona fide oncoprotein in human malignancies. CagA also elicits junctional and polarity defects in epithelial cells by interacting with and inhibiting partitioning-defective 1 (PAR1)/microtubule affinity-regulating kinase (MARK) independently of CagA tyrosine phosphorylation. Despite these CagA activities that contribute to neoplastic transformation, a causal link between CagA and *in vivo* oncogenesis remains unknown. Here, we generated transgenic mice expressing wild-type or phosphorylation-resistant CagA throughout the body or predominantly in the stomach. Wild-type CagA transgenic mice showed gastric epithelial hyperplasia and some of the mice developed gastric polyps and adenocarcinomas of the stomach and small intestine. Systemic expression of wild-type CagA further induced leukocytosis with IL-3/GM-CSF hypersensitivity and some mice developed myeloid leukemias and B cell lymphomas, the hematological malignancies also caused by gain-of-function SHP-2 mutations. Such pathological abnormalities were not observed in transgenic mice expressing phosphorylation-resistant CagA. These results provide first direct evidence for the role of CagA as a bacterium-derived oncoprotein (bacterial oncoprotein) that acts in mammals and further indicate the importance of CagA tyrosine phosphorylation, which enables CagA to deregulate SHP-2, in the development of *H. pylori*-associated neoplasms.

bacterial oncoprotein | transgenic mouse

Gastric adenocarcinoma is the fourth most common cancer and second leading cause of cancer-related death worldwide (1). Infection with *Helicobacter pylori* is the strongest risk factor for the development of gastric adenocarcinoma (2). *H. pylori* infection is also associated with mucosa-associated lymphoid tissue (MALT) lymphoma of B cell origin (3). *H. pylori is* subdivided into *cagA*-positive and *cagA*-negative strains and the *cagA*-positive strains are much more potent in induction of mucosal damage and severe atrophic gastritis (4, 5). Furthermore, epidemiological studies have suggested a critical role of *cagA*-positive *H. pylori* in the development of gastric adenocarcinoma (6, 7). The *cagA*-encoded CagA protein is delivered into gastric epithelial cells via the bacterial type IV secretion system (8), where it undergoes tyrosine phosphorylation by Src or Abl kinase at the Glu-Pro-Ile-Tyr-Ala (EPIYA) motifs present in variable numbers in the C-terminal region (9–12). Tyrosine-phosphorylated CagA then specifically binds to and aberrantly activates SHP-2 tyrosine phosphatase (9, 14), a bona fide oncoprotein whose gain-of-function mutations are associated with human malignancies (13). CagA-deregulated SHP-2 perturbs the Erk MAP kinase (15) and also dephosphorylates focal adhesion kinase (FAK) to induce an elongated cell-shape known as the hummingbird phenotype (8, 16). In addition, CagA interacts with Grb2 and c-Met in a phosphorylation-independent manner (17, 18) and Crk in a phosphorylation-dependent manner (19), which may have additional roles in the morphogenetic activity of CagA. More recently, CagA was found to impair the cell–cell interaction independently of CagA tyrosine phosphorylation. CagA disrupts tight junctions and causes the loss of apical-basolateral polarity in polarized epithelial cells by binding and inhibiting partitioning-defective 1 (PAR1)/microtubule affinity-regulating kinase (MARK) (20). CagA also destabilizes the E-cadherin/β-catenin complex, a major component of the adherens junctions, and thereby deregulates the β-catenin signal (21). Because normal epithelial architecture constrains abnormal cell proliferation (22), its disorganization by CagA may also contribute neoplastic transformation of cells.

Despite accumulating *in vitro* evidence for the transforming potential of CagA, the exact role of CagA in *in vivo* tumorigenesis remains obscure. Infection of wild-type mice with *H. pylori* does not result in the development of gastric carcinoma, probably because of poor host adaptation. Whereas long-term infection with *H. pylori* can induce gastric carcinoma in Mongolian gerbils, it remains uncertain whether CagA plays an active role in carcinogenesis in gerbils (23–25). Accordingly, rodent models have so far failed to demonstrate a causal link between CagA and the development of neoplasms *in vivo*.

In this work, we generated CagA transgenic mice and found that CagA induces abnormal proliferation of gastric epithelial cells and hematopoietic cells, followed by the development of gastrointestinal carcinomas and leukemias/lymphomas, in a tyrosine phosphorylation-dependent manner. Our findings reveal that *H. pylori* CagA is the first bacterial oncoprotein that acts in mammals.

Results

Synthesis and Analysis of the Humanized *cagA* Gene. Due to the structural polymorphism in the EPIYA-repeat region, individual CagA species show differential degrees of SHP-2-binding activity, which influences the magnitude of CagA virulence (8). We re-

Author contributions: M.H. designed research; N.O., H.Y., M. Miura, A.M., H.H., M. Musashi, and K.I. performed research; M.S., G.Y., and T.A. contributed new reagents/analytic tools; S.T. and H.S. analyzed data; and N.O., H.Y., M. Miura, A.M., H.H., and M.H. wrote the paper.

The authors declare no conflict of interest.

††To whom correspondence should be addressed. E-mail: mhata@igm.hokudai.ac.jp.

This article contains supporting information online at www.pnas.org/cgi/content/full/0711183105/DC1.

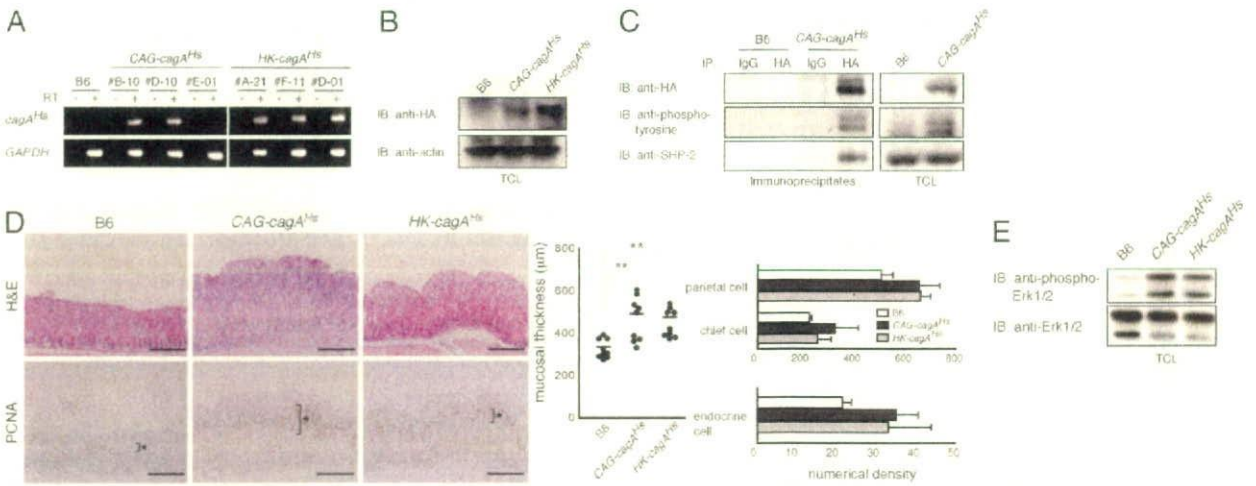

Fig. 1. Establishment of CagA transgenic mice. (*A*) $cagA^{Hs}$ mRNAs in the stomachs of 4-week-old $cagA^{Hs}$ heterozygous male mice as determined by RT-PCR. B6, C57BL/6J; RT, reverse transcription. *GAPDH* was used as a control. (*B*) Immunoblot analysis of CagA expression in the stomachs of 12-week-old B6, *CAG-cagA*^{Hs} (B-10), and *HK-cagA*^{Hs} (F-11) heterozygous male mice. IB, immunoblotting; TCL, total cell lysates. (*C*) Expression, tyrosine phosphorylation, and SHP-2-complex formation of CagA in embryonic fibroblasts prepared from B6 or *CAG-cagA*^{Hs} heterozygous mice (B-10). IP, immunoprecipitation. (*D*) Histological analysis of the glandular stomachs from 12-week-old B6, *CAG-cagA*^{Hs} (B-10), and *HK-cagA*^{Hs} (A-21) heterozygous male mice. *, PCNA-labeled cells. (Scale bars, 300 μm.) Mucosal thickness in the glandular stomach and numerical density of epithelial cells per millimeter of gastric mucosal height in these mice are shown. **, $P < 0.05$, Student's *t* test. Error bars indicate mean ± SD of triplicates. (*E*) Immunoblot analysis of Erk phosphorylation in gastric hyperplasia developed in $cagA^{Hs}$ mice.

ported that a CagA species possessing two repeated EPIYA-D segments (ABDD CagA) exhibits the greatest ability to bind and activate SHP-2 (26). Accordingly, we chose a *cagA* gene encoding ABDD CagA as the transgene in mice. The *H. pylori*-derived *cagA* gene is characterized by A/T-rich sequences, which could induce rapid gene silencing after integration into mammalian genomes [supporting information (SI) Fig. 5]. Also, *cagA* contains multiple ATTTA sequences that act as mRNA degradation motifs in mammalian cells (27). To avoid these potential problems, we chemically synthesized a DNA fragment encoding the entire ORF (3,729 base pairs) of ABDD CagA while converting bacterial *cagA* codons to those more commonly used in human genes, which significantly reduced the A/T contents and eliminated the ATTTA sequence (SI Fig. 5*B*). The synthesized DNA was then 3′-tagged with a sequence encoding the hemagglutinin (HA) to generate the humanized *cagA* gene ($cagA^{Hs}$). Expectedly, transfection of a $cagA^{Hs}$ expression vector gave rise to higher levels of CagA expression and greater magnitude for induction of cells with the hummingbird phenotype than did a bacterial *cagA* vector in AGS human gastric epithelial cells (SI Fig. 6).

Generation of Transgenic Mice Bearing Humanized *cagA* Gene. To express CagA systemically in mice, $cagA^{Hs}$ was connected downstream of the chicken *β-actin* and *globin* fusion promoter (*CAG* promoter) (28). The $cagA^{Hs}$ DNA was also connected downstream of the *β subunit* gene promoter of mouse H^+/K^+-*ATPase* (*HK* promoter) (29), with the expectation of predominant expression of CagA in the stomach (SI Fig. 7*A*). After injection of the transgenic constructs into fertilized mouse eggs, three lines (B-10, D-10, and E-01) of the *CAG* promoter-driven $cagA^{Hs}$ (*CAG-cagA*^{Hs}) transgenic mice and three lines (A-21, F-11, and D-01) of the *HK* promoter-driven $cagA^{Hs}$ (*HK-cagA*^{Hs}) transgenic mice were established (SI Fig. 7*B*). These $cagA^{Hs}$ mice were indistinguishable from the wild-type littermates in behavior and weight when they were born, and they developed normally. No overt difference was found between $cagA^{Hs}$ heterozygous and homozygous mice.

In *CAG-cagA*^{Hs} mice, $cagA^{Hs}$ mRNAs were detected in various organs and tissues with high levels of expression in the stomach, ileum, colon, brain, lung, thymus, and testis (Fig. 1*A* and SI Fig. 8*A*). In *HK-cagA*^{Hs} mice, $cagA^{Hs}$ mRNAs were predominantly expressed in the stomach. However, significant amounts of $cagA^{Hs}$ transcripts were also present in other tissues such as the lung, intestine, thymus, spleen, and testis, indicating leaky transcription from the transgenic *HK* promoter (Fig. 1*A* and SI Fig. 8 *A* and *B*). Expression of the CagA protein was confirmed in tissue extracts prepared from the stomachs of 4-week-old *CAG-cagA*^{Hs} and *HK-cagA*^{Hs} transgenic mice (Fig. 1*B*), although the levels were much lower than those of gastric epithelial cells transfected with CagA-expression vector or *in vitro* infected with *cagA*-positive *H. pylori* (data not shown). Analysis of embryonic fibroblasts from *CAG-cagA*^{Hs} mice confirmed tyrosine phosphorylation of CagA and complex formation of CagA with SHP-2 (Fig. 1*C*).

Gastrointestinal Abnormalities in Wild-type CagA Transgenic Mice. At 12 weeks of age, mice were killed and autopsies revealed a broad thickening of gastric mucosa, primarily at the body of the stomach, in both the *CAG-cagA*^{Hs} and *HK-cagA*^{Hs} mice, although the penetrance of this mucosal change was incomplete (Fig. 1*D* and SI Fig. 9). This may be attributable to the differences in CagA levels among individual transgenic mice even though they are genetically identical. Histologically, the change was due to epithelial hyperplasia of the glandular stomach, in which the proliferative zone in the gastric gland was markedly expanded, and was concomitantly associated with increased numbers of parietal, chief, and endocrine cells, which were all derived from precursors present in the proliferative zone (Fig. 1*D*). In the hyperplastic lesion, CagA expression was concomitantly associated with the hyperactivation of the Erk MAP kinase, a downstream effector of CagA-deregulated SHP-2 (Fig. 1*E*) (15).

At 48 weeks of age, several *CAG-cagA*^{Hs} and *HK-cagA*^{Hs} mice had developed polyps in the glandular stomach. These polyps were mostly hyperplastic polyps, consisting of surface epithelial cells with limited atypical cellularity without nuclear pseudostratification. By 72 weeks of age, 15 of 184 *CAG-cagA*^{Hs}/line B-10 mice, 8 of 35 *CAG-cagA*^{Hs}/line D-10 mice and 5 of 98 *HK-cagA*^{Hs}/line A-21 mice had developed hyperplastic polyps (Fig. 2*A* and SI Table 1). Furthermore, a small number of $cagA^{Hs}$ mice at 72 weeks of age had developed adenocarcinomas, two in the stomach and four in the small intestine (five in *CAG-cagA*^{Hs}/line B-10 and 1 in *HK-cagA*^{Hs}/line F-11) (Fig. 2 *B* and *C* and SI Table 1). These

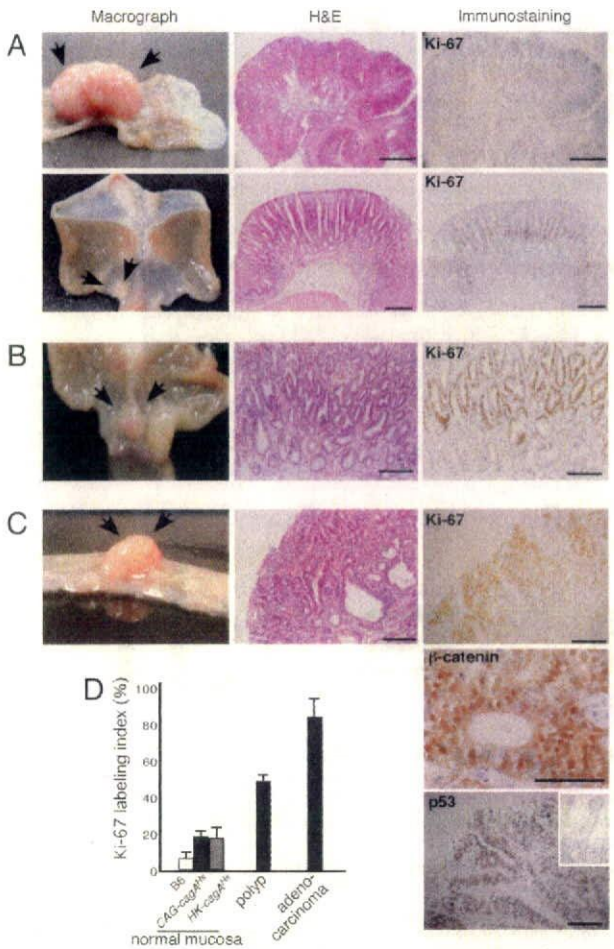

Fig. 2. Gastrointestinal polyps and adenocarcinomas in *cagA*^{Hs} mice. Histological analysis of H&E staining and immunostaining. (*A*) Hyperplastic polyps developed in the stomachs of 72-week-old *CAG-cagA*^{Hs} (B-10) homozygous female mice (*Upper*) and *HK-cagA*^{Hs} (A-21) heterozygous male (*Lower*) mice. Scale bars, 300 μm. (*B*) Adenocarcinoma developed in the stomach of a 72-week-old *CAG-cagA*^{Hs} homozygous male mouse (B-10). Scale bars, 100 μm. (*C*) Adenocarcinoma developed in the small intestine of a 72-week-old *CAG-cagA*^{Hs} heterozygous male mouse (B-10). In the p53-immunostaining panel, matched control is shown in *Inset*. (Scale bars, 100 μm.) (*D*) Ki-67 labeling indexes of gastric lesions in *cagA*^{Hs} mice. Error bars indicate mean ± SD.

carcinomas consisted of irregular branching glands lined by atypical columnar cells that showed plump nuclei with large nucleoli and high mitotic index (SI Fig. 10*A*). The high proliferating activity of the tumors was confirmed by Ki-67 immunostaining (Fig. 2 *C* and *D*). In several cases, neoplastic glands had penetrated the lumina muscularis mucosa (SI Fig. 10*B*). Immunostaining of the tumor specimens demonstrated intense nuclear positivity of p53 and β-catenin in intestinal adenocarcinomas, suggesting mutations in the *β-catenin* and/or *Apc* and *p53* genes in the neoplastic lesions but not in gastric adenocarcinomas (Fig. 2*C* and data not shown). These findings indicate the requirement of cell type-specific secondary events for the development of gastrointestinal neoplasms. No gastrointestinal polyps or tumors were found in the wild-type littermate mice by 72 weeks after birth with continual observation (n = 100).

It has been generally believed that atrophic gastritis and intestinal metaplasia, a transdifferentiation of gastric epithelial cells to an intestinal phenotype, are precancerous gastric mucosal changes, from which intestinal-type gastric adenocarcinoma arises (30). We therefore performed histological examination of gastric mucosa from 72-week-old *cagA*^{Hs} mice but did not find any signs of pathological abnormalities (data not shown). From these observations, we concluded that CagA has the ability to induce epithelial hyperplasia, polyps, and adenocarcinomas in the stomach, without causing overt inflammation or intestinal metaplasia. We also note that no overt histopathological abnormalities were found in the intestinal tract of *cagA*^{Hs} mice without tumors.

Hematopoietic Abnormalities in Wild-Type CagA Transgenic Mice. In addition to the gastrointestinal abnormalities, some of the *cagA*^{Hs} mice had developed hematopoietic malignancies by 72 weeks of age (16 of 152 in *CAG-cagA*^{Hs}/line B-10; 1 of 77 in *HK-cagA*^{Hs}/line A-21; and 1 of 38 in *HK-cagA*^{Hs}/line F-11) (SI Table 1). It should be noted here that CagA was also expressed in the spleen of *HK-cagA*^{Hs} mice (SI Fig. 8*B*). The leukemic mice showed marked splenomegaly, and immunohistochemical analyses of the spleens revealed that they were of myeloid (5 cases), B cell (12 cases), or T cell (1 case) origin (Fig. 3 *A–C*). Mild leukocytosis (granulocytosis) was also found in the peripheral blood of 72-week-old *cagA*^{Hs} mice without hematological malignancies (Fig. 3*D*). No age-matched wild-type littermate mice developed hematological abnormality (n = 100).

The observed spectrum of hematological malignancies in CagA transgenic mice was similar to that evoked by gain-of-function SHP-2 mutations (13). We thus suspected that CagA-deregulated SHP-2 is also involved in the transformation of hematopoietic cells as well. Indeed, in spleen cells from *cagA*^{Hs} mice, the Erk MAP kinase was again hyperactivated (Fig. 3*E*). Because SHP-2 potentiates cellular responses to interleukin (IL)-3 and granulocyte-macrophage colony-stimulating factor (GM-CSF) (31), we performed a colony assay to evaluate activation status of SHP-2. Bone marrow cells from *cagA*^{Hs} mice showed hypersensitivity to IL-3 and GM-CSF and also exhibited spontaneous colony formation in the absence of cytokines (Fig. 3*F*). These observations are consistent with the idea that SHP-2 is deregulated in *cagA*^{Hs} mice and suggest that CagA-deregulated SHP-2 plays a key role in the abnormal proliferation of multiple hematopoietic cells.

Role of Tyrosine Phosphorylation in the *in Vivo* Pathogenic Activity of CagA. Tyrosine-phosphorylated CagA specifically binds to and deregulates SHP-2. To explore the role of CagA tyrosine phosphorylation in the development of gastrointestinal and hematopoietic lesions observed in *cagA*^{Hs} mice, we next generated a *PR-cagA*^{Hs} gene encoding a phosphorylation-resistant ABDD CagA (PR-CagA), which cannot bind SHP-2, from *cagA*^{Hs} (SI Fig. 11 *A* and *B*). Transgenic constructs were made by connecting the *PR-cagA*^{Hs} DNA fragment downstream of the *CAG* or *HK* promoter (SI Fig. 11*C*). After injection of the transgenic constructs into fertilized mouse eggs, three lines each for the *CAG* promoter-driven *PR-cagA*^{Hs} (*CAG-PR-cagA*^{Hs}) and *HK* promoter-driven *PR-cagA*^{Hs} (*HK-PR-cagA*^{Hs}) transgenic mice were established (Fig. 4*A*). Systemic expression of *PR-cagA*^{Hs} in *CAG-PR-cagA*^{Hs} mice was confirmed by RT-PCR analysis (SI Fig. 11*D*). Again, expression of *PR-cagA*^{Hs} in *HK-PR-cagA*^{Hs} mice was not specific to the stomach.

Despite significantly higher levels of PR-CagA expression than those of wild-type CagA in transgenic mice (Fig. 4 *B* and *C*), *PR-cagA*^{Hs} mice neither showed gastric epithelial hyperplasia or leukocytosis nor developed neoplasms (except one case of gastric hyperplastic polyp in a *HK-PR-cagA*^{Hs} mouse) (Fig. 4 *D* and *E*, SI Fig. 11*E*, and SI Table 1). Furthermore, bone marrow cells from *PR-cagA*^{Hs} mice did not show hypersensitivity to IL-3 or GM-CSF (Fig. 4*F*). These observations indicate that tyrosine-phosphorylated CagA, which enables CagA to bind SHP-2, plays an important role in the abnormal proliferation of gastric epithelial and hematopoietic cells and subsequent development of neoplasms.

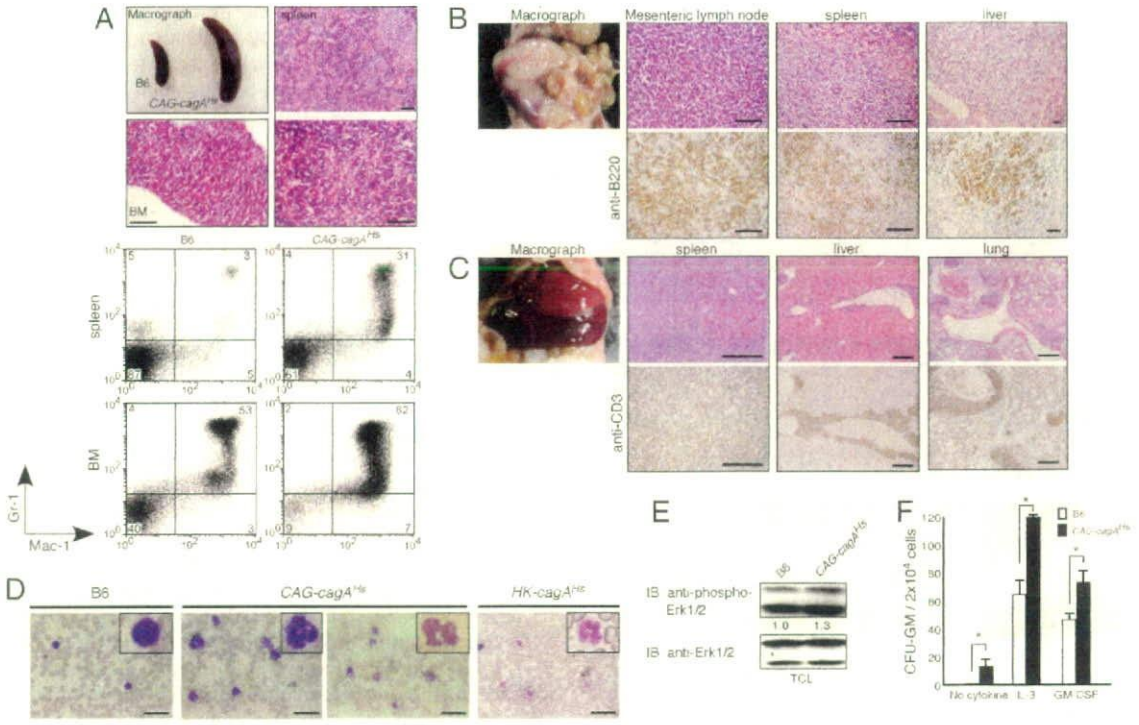

Fig. 3. Hematological abnormalities in *cagA*^{Hs} mice. (*A*) Myeloid leukemia developed in a 72-week-old *CAG-cagA*^{Hs} heterozygous male mouse (B-10). (*Upper*) Macroscopic and histological views of the spleen and bone marrow (BM) from the mouse with leukemia. Age-matched control B6 spleen is also shown. (Scale bars, 100 μm.) (*Lower*) FACS analyses of spleen and BM cells from the mice with leukemias. Cells were double-stained with anti-Gr-1 and anti-Mac-1 antibodies, showing increased numbers of Mac-1/Gr-1-double-positive myeloid cells. The percentage of each cell population is indicated. BM cells from B6 mice were used as a control. (*B*) B cell lymphoma of mesenteric lymph-node origin developed in a 72-week-old *CAG-cagA*^{Hs} (B-10) heterozygous male mice. Macroscopic view, H&E staining, and anti-B220 immunostaining showing diffuse infiltration of B cells into the spleen and liver, resembling diffuse large B cell lymphoma. (Scale bars, 100 μm.) (*C*) T cell lymphoma developed in a 72-week-old *CAG-cagA*^{Hs} (B-10) homozygous male mice. Macroscopic view, H&E staining and anti-CD3 immunostaining showing infiltration of T cells into the spleen, liver, and lung. (Scale bars, 300 μm.) (*D*) Blood smears from 72-week-old B6, *CAG-cagA*^{Hs} (B-10) and *HK-cagA*^{Hs} (F-11) heterozygous male mice, showing increased granulocytes in *cagA*^{Hs} mice. (Scale bars, 30 μm.) (*E*) Immunoblot analysis of Erk phosphorylation in spleen cells from B6 or *CAG-cagA*^{Hs} (B-10) mice. (*F*) Myeloid colonies derived from bone marrow cells of 72-week-old B6 or *CAG-cagA*^{Hs} (B-10) heterozygous male mice with no evidence of hematopoietic malignancies. Error bars indicate mean ± SD of triplicates. *, $P < 0.05$, Student's *t* test.

Discussion

In this work, we generated CagA transgenic mice in which involvement of other bacterial factors in pathogenesis is totally excluded, and we obtained formal evidence that CagA is a bacterial oncoprotein, the expression of which suffices for development of neoplasms. Despite systemic expression in mice, CagA exhibits oncogenic actions specifically toward gastrointestinal and hematopoietic cells. Because the tumor formation depends on CagA tyrosine phosphorylation, the observed tissue-specific oncogenic action of CagA might reflect the differential activation status of CagA kinases, such as Src and Abl, in different cell lineages. Furthermore, given that CagA tyrosine phosphorylation is an essential prerequisite for the interaction of CagA with SHP-2 oncoprotein (9, 14), our results point to the importance of CagA-deregulated SHP-2 in *in vivo* tumorigenesis.

SHP-2 is required for normal development of both myeloid and lymphoid lineage cells (32, 33), and gain-of-function mutations of SHP-2 are associated with childhood leukemias (13, 33, 34). We found in this work that bone marrow cells from *cagA*^{Hs} mice exhibit hypersensitivity to IL-3 and GM-CSF, the hallmark of SHP-2 activation (31, 35). The finding provides evidence for the hyperactivation of SHP-2 in *cagA*^{Hs} mice and suggests the role of CagA-deregulated SHP-2 in leukemogenesis. This in turn raises the possibility that CagA is also involved in the development of *H. pylori*-associated B cell MALT lymphoma, although the association of *cagA*-positive *H. pylori* with MALT lymphoma is still controversial (3, 4, 36). It would be interesting to know whether CagA can be delivered into B cells that migrate to the *H. pylori*-infected stomach.

Whereas *cagA*^{Hs} mice develop both gastrointestinal and hematopoietic malignancies, SHP-2 mutation is rarely found in solid tumors (37). Also, notably, mice systemically expressing a gain-of-function SHP-2 mutant developed myeloproliferative disease but not solid tumors (35). These observations suggest that development of gastrointestinal tumors in *cagA*^{Hs} mice, which still depends on CagA tyrosine phosphorylation, requires additional CagA activities that cooperate with CagA-deregulated SHP-2. An intriguing idea is that phosphorylation-independent interaction of CagA with PAR1, which inhibits PAR1 kinase activity and thereby causes junctional and polarity defects in epithelial cells (20), is also involved the development of solid tumors. Indeed, the connection between epithelial cell polarity and tumors has been provided by the works of *Drosophila* tumor suppressor genes such as *dlg*, *lgl*, and *scribble* (22, 38). Also notably, PAR1 is a downstream target of LKB1/PAR4 kinase, loss-of-function mutations of which lead to the gastrointestinal cancer-prone Peutz–Jeghers syndrome (39).

The rare and delayed appearance of neoplasms in *cagA*^{Hs} mice indicates a weak oncogenic potential of CagA quantitatively and/or qualitatively. Nevertheless, the efficiency of tumors developed among different strains of *cagA*^{Hs} mice was still correlated with the levels of CagA expressed. Notably, expression of wild-type CagA was significantly lower than that of PR-CagA in transgenic mice, possibly because robust activation of SHP-2 by high levels of

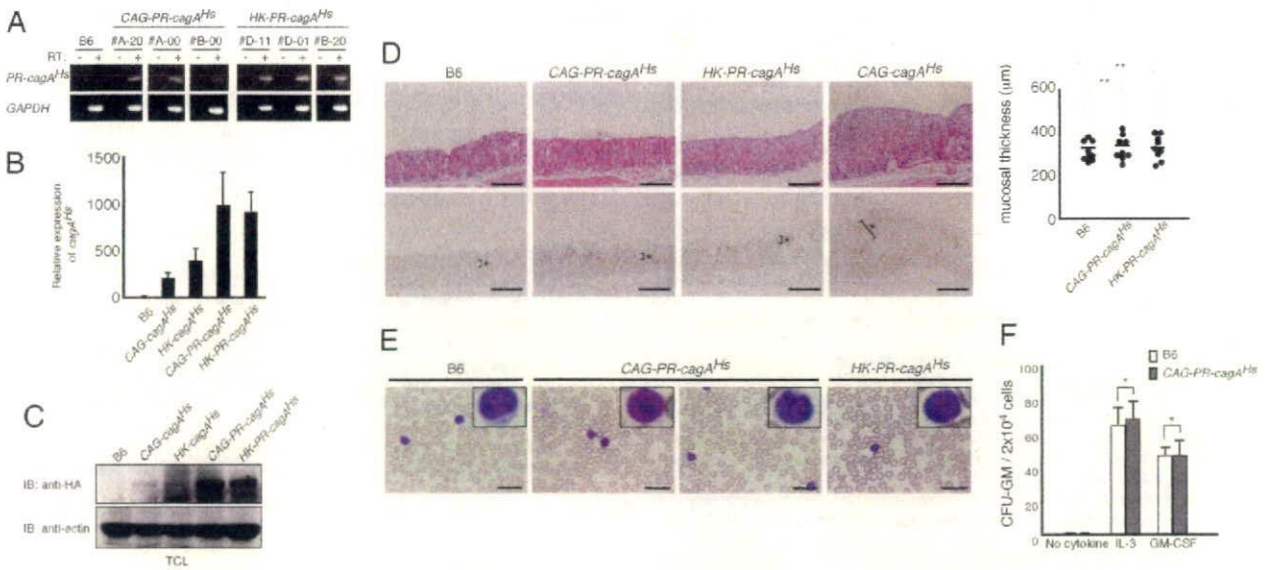

Fig. 4. Analysis of transgenic mice expressing phospho-resistant (PR) CagA. (*A*) *PR-cagA*^{Hs} mRNAs in the stomachs of 12-week-old *PR-cagA*^{Hs} heterozygous male mice as determined by RT-PCR analysis. (*B*) Relative *cagA*^{Hs} mRNA levels in the stomachs of 12-week-old B6, *CAG-cagA*^{Hs} (B-10), *HK-cagA*^{Hs} (A-21), *CAG-PR-cagA*^{Hs} (A-20), and *HK-PR-cagA*^{Hs} (D-01) heterozygous male mice. Error bars indicate mean ± SD of triplicates. (*C*) Immunoblot analysis of CagA expression in the stomachs of 12-week-old B6, *CAG-cagA*^{Hs} (B-10), *HK-cagA*^{Hs} (A-21), *CAG-PR-cagA*^{Hs} (A-20), and *HK-PR-cagA*^{Hs} (D-01) heterozygous male mice. (*D*) H&E staining and anti-PCNA immunostaining of the glandular stomachs from 12-week-old B6, *CAG-PR-cagA*^{Hs} (A-20), *HK-PR-cagA*^{Hs} (D-01), and *CAG-cagA*^{Hs} (B-10) heterozygous male mice. *, PCNA-labeled cells. (Scale bars, 300 μm.) Gastric mucosal thicknesses of these mice are shown at *Right*. **, $P > 0.05$, Student's *t* test. (*E*) Blood smears from 72-week-old B6, *CAG-PR-cagA*^{Hs} (A-20), and *HK-PR-cagA*^{Hs} (B-20) heterozygous male mice. (*F*) Myeloid colonies derived from bone marrow cells of 72-week-old B6 or *CAG-PR-cagA*^{Hs} (A-20) heterozygous male mice with no evidence of hematopoietic malignancies. Error bars indicate mean ± SD of triplicates. *, $P > 0.05$, Student's *t* test.

wild-type CagA is not tolerated during embryogenesis as suggested (35). Such a quantitative restriction on wild-type CagA expression could explain at least in part the low incidence of neoplasms in *cagA*^{IIs} mice. Intriguingly, *cagA*^{IIs} mice develop gastric epithelial hyperplasia and tumors in the absence of overt mucosal inflammation or metaplastic change. This finding suggests that the oncogenic potential of CagA is cell-autonomous and that development of gastric carcinoma does not necessarily require chronic inflammation and presumed precancerous conditions, such as intestinal metaplasia. Obviously, however, the notion does not exclude the possibility that host responses to *H. pylori* infection, such as production of a variety of inflammatory cytokines, potentiate the weak oncogenic activity of CagA. It is also possible that low levels of CagA elicits gastric epithelial cell proliferation, whereas high levels of CagA triggers apoptosis, possibly by inducing oncogenic stress as described (14–16).

Once established, maintenance of the transformed phenotype of gastric adenocarcinoma no longer requires CagA. Hence, whereas CagA plays a critical role during the early steps of gastric carcinogenesis, populations of preneoplastic cells that undergo continuous CagA exposure may progress to spawn cell variants that acquire additional oncogenic changes, such as those involved in the SHP-2/Ras/Erk pathway, and/or apoptotic regulation, such as p53, as shown in the CagA-induced intestinal carcinoma, which compensate CagA functions and thereby confer CagA-independence during the later phases of carcinogenesis.

Our study establishes a causal relationship between *H. pylori* CagA and tumorigenesis and suggests that CagA is a critical molecular target for therapeutic application to *H. pylori*-associated neoplasms.

Materials and Methods

Transgenic Mice. Chemically synthesized *cagA*^{Hs} DNA was subcloned into pCAGGS (28) or pHKATP vector (29). The *CAG-cagA*^{Hs} or *HK-cagA*^{Hs} fragment consisting of the promoter, *cagA*^{Hs} and polyA cassettes derived from β-*globin* gene was excised from the resulting plasmid by restriction enzyme digestion, and then injected directly into fertilized eggs of C57BL/6J mice. Transgenic mice were identified by PCR analysis of tail DNAs, using *cagA*^{Hs}-specific primers (*cagA*^{Hs}-forward 5′-CACAATAACGCTCTGTCATCAGTGCTG-3′, *cagA*^{Hs}-reverse 5′-TCAACGTATAAGACACTTCCCCATTGC-3′). PCR amplification was performed at 94°C for 5 min, 94°C for 30 seconds, 62°C for 30 seconds, 72°C for 30 seconds (30 cycles), and 72°C for 7 min. All of the animal experiments were carried out according to the protocol approved by the Ethics Committee for Animal Experiments at Hokkaido University.

RT-PCR and Quantitative RT-PCR. Total RNA was extracted from mouse tissues with the use of TRIzol Reagent (Invitrogen). Quantitative RT-PCR was performed by using SYBR Green fluorescence detection system (Qiagen) with ABI PRISM 7700 sequencer (Applied Biosystems). The following primer pairs were used for PCR amplification: *cagA*^{Hs}-forward: 5′-AAGCTGCTTCTGCGATTAACCG-3′, *cagA*^{Hs}-reverse: 5′-GGAGTCTTTCAGTTCGTC-3′, *GAPDH*-forward: 5′-ACCACAGTCCATGCCATCAC-3′, and *GAPDH*-reverse: 5′-TCCACCACCCTGTTGCTGTA-3′.

Immunoprecipitation and Immunoblotting. Protein extracts prepared from tissues or cells were subjected to immunoprecipitation or immunoblotting with an anti-HA antibody (3F10; Roche) as described in ref. 9.

Histopathological Analyses. Tissue specimens were fixed in formalin, embedded in paraffin, sectioned, and stained with hematoxylin and eosin (H&E). Thickness of gastric mucosa was evaluated by measuring three distinct points of the glandular stomach for each mouse. Cancer diagnosis was made based on Ki-67 labeling index, nuclear atypia, and mitosis counts by two independent pathologists (S.T. and H.S.). For immunohistochemical staining, sections were deparaffinized, rehydrated, and then incubated with anti-PCNA (PC10; Dako), anti-Ki-67 (Dako), anti-B220 (RA3–6B2), anti-p53 (CM5; Novocastra), anti-CD3 (Dako), or anti-β-catenin antibody (BD Bioscience). Sections were then washed and incubated with appropriate secondary antibodies. Reacted antibodies were detected by the peroxydase reaction, using diaminobenzidine as substrate. Chief cells were identified by H&E staining. Parietal cells and endocrine cells were identified by immunostaining with anti-H^+/K^+-ATPase α-subunit antibody (Chemicon) and anti- chromogranin A antibody (Dako), respectively. Peripheral blood smears were stained with May–Giemsa solution.

Flow Cytometry. Cells were washed in PBS containing 0.5% BSA and 0.05% NaN_3. Fc receptor-mediated binding was blocked by preincubation of cells with supernatants of 2.4G2 hybridoma. Fluorescence isothiocyanate (FITC)-anti-Gr-1 and phycoerythrin (PE)-anti-CD11b (Mac-1) antibodies were purchased from BD Bioscience. Flow cytometric analysis was performed by using FACSCalibur (Becton–Dickinson) and analyzed with CellQuest software.

Colony Assay. Methylcellulose cell culture was performed in 35-mm culture dishes as described in ref. 40.

Statistical Analysis. Statistical analysis was performed by using Student's *t* test, the χ^2 test, or Fisher's exact test.

ACKNOWLEDGMENTS. We thank J. I. Gordon for pHKATP-hGH1, K. Shimizu and Y. Shibuta for technical assistance, and K. Nagashima and S. Kon for advice. This work was supported by Grants-in-Aid for Scientific Research from the Ministry of Education, Culture, Sports, Science and Technology of Japan and by a Takeda Science Foundation Research Grant (to M.H.). N.O. is a Japan Society for the Promotion of Science Research Fellow.

1. Parkin DM (2001) Global cancer statistics in the year 2000. *Lancet Oncol* 2:533–543.
2. Peek RM, Jr, Blaser MJ (2002) *Helicobacter pylori* and gastrointestinal tract adenocarcinomas. *Nat Rev Cancer* 2:28–37.
3. Parsonnet J, *et al.* (1994) *Helicobacter pylori* infection and gastric lymphoma. *N Engl J Med* 330:1267–1271.
4. Kuipers EJ, Perez-Perez GI, Meuwissen SG, Blaser MJ (1995) *Helicobacter pylori* and atrophic gastritis: importance of the *cagA* status. *J Natl Cancer Inst* 87:1777–1780.
5. Sozzi M, *et al.* (1998) Atrophic gastritis and intestinal metaplasia in *Helicobacter pylori* infection: the role of CagA status. *Am J Gastroenterol* 93:375–379.
6. Blaser MJ, *et al.* (1995) Infection with *Helicobacter pylori* strains possessing *cagA* is associated with an increased risk of developing adenocarcinoma of the stomach. *Cancer Res* 55:2111–2115.
7. Parsonnet J, Friedman GD, Orentreich N, Vogelman H (1997) Risk for gastric cancer in people with CagA positive or CagA negative *Helicobacter pylori* infection. *Gut* 40:297–301.
8. Segal ED, Cha J, Lo J, Falkow S, Tompkins LS (1999) Altered states: Involvement of phosphorylated CagA in the induction of host cellular growth changes by *Helicobacter pylori*. *Proc Natl Acad Sci USA* 96:14559–14564.
9. Higashi H, *et al.* (2002) SHP-2 tyrosine phosphatase as an intracellular target of *Helicobacter pylori* CagA protein. *Science* 295:683–686.
10. Higashi H, *et al.* (2002) Biological activity of the *Helicobacter pylori* virulence factor CagA is determined by variation in the tyrosine phosphorylation sites. *Proc Natl Acad Sci USA* 99:14428–14433.
11. Selbach M, Moese S, Hauck CR, Meyer TF, Backert S (2002) Src is the kinase of the *Helicobacter pylori* CagA protein *in vitro* and *in vivo*. *J Biol Chem* 277:6775–6778.
12. Poppe M, Feller SM, Römer G, Wessler S (2007) Phosphorylation of *Helicobacter pylori* CagA by c-Abl leads to cell motility. *Oncogene* 26:3462–3472.
13. Tartaglia M, Gelb BD (2005) Germ-line and somatic *PTPN11* mutations in human disease. *Eur J Med Genet* 48:81–96.
14. Hatakeyama M (2004) Oncogenic mechanisms of the *Helicobacter pylori* CagA protein. *Nat Rev Cancer* 4:688–694.
15. Higashi H, *et al.* (2004) *Helicobacter pylori* CagA induces Ras-independent morphogenetic response through SHP-2 recruitment and activation. *J Biol Chem* 279:17205–17216.
16. Tsutsumi R, Takahashi A, Azuma T, Higashi H, Hatakeyama M (2006) Focal adhesion kinase is a substrate and downstream effector of SHP-2 complexed with *Helicobacter pylori* CagA. *Mol Cell Biol* 26:261–276.
17. Churin Y, *et al.* (2003) *Helicobacter pylori* CagA protein targets the c-Met receptor and enhances the motogenic response. *J Cell Biol* 161:249–255.
18. Mimuro H, *et al.* (2002) Grb2 is a key mediator of *Helicobacter pylori* CagA protein activities. *Mol Cell* 10:745–755.
19. Suzuki M, *et al.* (2005) Interaction of CagA with Crk plays an important role in *Helicobacter pylori*-induced loss of gastric epithelial cell adhesion. *J Exp Med* 202:1235–1247.
20. Saadat I, *et al.* (2007) *Helicobacter pylori* CagA targets PAR1/MARK kinase to disrupt epithelial cell polarity. *Nature* 447:330–333.
21. Murata-Kamiya N, *et al.* (2007) *Helicobacter pylori* CagA interacts with E-cadherin and deregulates the β-catenin signal that promotes intestinal transdifferentiation in gastric epithelial cells. *Oncogene* 26:4617–4626.
22. Bilder D (2004) Epithelial polarity and proliferation control: links from the *Drosophila* neoplastic tumor suppressors. *Genes Dev* 18:1909–1925.
23. Honda S, *et al.* (1998) Development of *Helicobacter pylori*-induced gastric carcinoma in Mongolian gerbils. *Cancer Res* 58:4255–4259.
24. Watanabe T, Tada M, Nagai H, Sasaki S, Nakao M (1998) *Helicobacter pylori* infection induces gastric cancer in Mongolian gerbils. *Gastroenterology* 115:642–648.
25. Rieder G, Merchant JL, Haas R (2005) *Helicobacter pylori* cag-type IV secretion system facilitates corpus colonization to induce precancerous conditions in Mongolian gerbils. *Gastroenterology* 128:1229–1242.
26. Naito M, *et al.* (2006) Influence of EPIYA-repeat polymorphism on the phosphorylation-dependent biological activity of *Helicobacter pylori* CagA. *Gastroenterology* 130:1181–1190.
27. Ross J (1996) Control of messenger RNA stability in higher eukaryotes. *Trends Genet* 12:171–175.
28. Araki K, Araki M, Miyazaki J, Vassalli P (1995) Site-specific recombination of a transgene in fertilized eggs by transient expression of Cre recombinase. *Proc Natl Acad Sci USA* 92:160–164.
29. Lorenz RG, Gordon JI (1993) Use of transgenic mice to study regulation of gene expression in the parietal cell linage of gastric units. *J Biol Chem* 268:26559–26570.
30. Correa P (1992) Human gastric carcinogenesis: a multistep and multifactorial process–First American Cancer Society Award Lecture on Cancer Epidemiology and Prevention. *Cancer Res* 52:6735–6740.
31. Schubbert S, *et al.* (2005) Functional analysis of leukemia-associated *PTPN11* mutations in primary hematopoietic cells. *Blood* 106:311–317.
32. Qu CK, *et al.* (1997) A deletion mutation in the SH2-N domain of Shp-2 severely suppresses hematopoietic cell development. *Mol Cell Biol* 17:5499–5507.
33. Qu CK, Nguyen S, Chen J, Feng GS (2001) Requirement of Shp-2 tyrosine pohosphatase in lymphoid and hematopoietic cell development. *Blood* 97:911–914.
34. Tartaglia M, *et al.* (2003) Somatic mutations in *PTPN11* in juvenile myelomonocytic leukemia, myelodysplastic syndromes and acute myeloid leukemia. *Nat Genet* 34:148–150.
35. Araki T, *et al* (2004) Mouse model of Noonan syndrome reveals cell type- and gene dosage-dependent effects of *Ptpn11* mutation. *Nat Med* 10:849–857.
36. De Jong D, *et al.* (1996) Gastric non-Hodgkin lymphomas of mucosa-associated lymphoid tissue are not associated with more aggressive *Helicobacter pylori* strains as identified by CagA. *Am J Clin Pathol* 106:670–675.
37. Bentires-Alj M, *et al.* (2004) Activating mutations of the noonan syndrome-associated *SHP2/PTPN11* gene in human solid tumors and adult acute myelogenous leukemia. *Cancer Res* 64:8816–8820.
38. Humbert P, Russell S, Richardson H (2003) Dlg, Scribble and Lgl in cell polarity, cell proliferation and cancer. *Bioessays* 25:542–553.
39. Alessi DR, Sakamoto K, Bayascas JR (2006) LKB1-dependent signaling pathways. *Annu Rev Biochem* 75:137–163.
40. Musashi M, *et al.* (1991) Phorbol ester enhancement of IL-3-dependent proliferation of primitive hematopoietic progenitors of mice. *J Pharmacol Exp Ther* 280:225–231.

research articles Journal of proteome research

Proteomics- and Transcriptomics-Based Screening of Differentially Expressed Proteins and Genes in Brain of Wig Rat: A Model for Attention Deficit Hyperactivity Disorder (ADHD) Research

Misato Hirano,[†] Randeep Rakwal,*[,†] Junko Shibato,[†] Hirofumi Sawa,[‡] Kazuo Nagashima,[‡] Yoko Ogawa,[§] Yasukazu Yoshida,[§] Hitoshi Iwahashi,[§] Etsuo Niki,[§] and Yoshinori Masuo[†]

Human Stress Signal Research Center (HSS), National Institute of Advanced Industrial Science and Technology (AIST), Tsukuba West, 16-1 Onogawa, Tsukuba 305-8569, Japan, Hokkaido University, Sapporo 060-8638, Japan, and HSS, AIST Kansai Center, 1-8-31, Midorigaoka, Ikeda 563-8577, Japan

Received January 12, 2008

Two global omics approaches were applied to develop an inventory of differentially expressed proteins and genes in Wig rat, a promising animal model of attention-deficit hyperactivity disorder (ADHD). The frontal cortex, striatum, and midbrain of Wig rat at 4 weeks of age were dissected for proteomics and transcriptomics analyses. Two-dimensional gel electrophoresis detected 13, 1, and 16 differentially expressed silver nitrate-stained spots in the frontal cortex, striatum, and midbrain, respectively. Peptide mass fingerprinting/tandem mass spectrometry identified 19 nonredundant proteins, belonging to 7 functional categories, namely, signal transduction, energy metabolism, cellular transport, protein with binding function, protein synthesis, cytoskeleton, and cell rescue. Interestingly, 10 proteins that were indentified in the present study were also previously reported in studies involving neurodegenerative diseases and psychiatric disorders, such as Alzheimer's disease (AD), Parkinson's disease, and Schizophrenia. Moreover, some of the proteins identified in the midbrain were involved in synaptic vesicular transport, suggesting abnormality in neurotransmitter release in this region. On the other hand, transcriptomics analysis of combined frontal cortex, striatum, and midbrain by rat whole genome 44K DNA oligo microarray revealed highly up-regulated (28) and down-regulated (33) genes. Functional categorization of these genes showed cellular transport, metabolism, protein fate, signal transduction, and transcription as the major categories, with 26% genes of unknown function. Some of the identified genes were related to AD, fragile X syndrome, and ADHD. This is a first comprehensive study providing insight into molecular components in Wig rat brain, and will help to elucidate the roles of identified proteins and genes in Wig rat brain, hopefully leading to uncovering the pathogenesis of ADHD.

Keywords: Gel-based proteomics • Wig • ADHD • brain regions • biomarkers • neurodegenerative diseases

1. Introduction

Patients with attention-deficit hyperactivity disorder (ADHD) show motor hyperactivity under inappropriate situations, especially during childhood. A potential pathogenesis of ADHD results in abnormality in the development of dopamine (DA) neuron; however, the etiology of this developmental disorder is unknown (reviewed in ref 1). Various studies have focused on investigating the mechanism of ADHD using animal models (reviewed in refs 2 and 3). Wiggling (Wig) Wistar King Aptekman/Hokkaido (WKAH) rats were recently designated from a strain of the Long-Evans Cinnamon (LEC) as a new rat model of ADHD.[4] The Wig rats show motor abnormalities such as "wiggling" movement, a kind of circular movement with head shaking induced by stimulation. This single detailed behavioral study revealed that Wig rats at 12−14 weeks of age show hyperactivity, impaired working memory and impulsive behavior, as demonstrated by motor activity and the open-field and Y-maze tests.[4] It was also reported that these abnormalities are transmitted by a single autosomal recessive gene with Mendelian pattern. These characteristics make the Wig rat a possible animal model of human ADHD.

With a model in place, the next logical step was to analyze it further, and for this, Wig rats at 4−5 weeks of age, the juvenile period, were used in the present study. The reason for selecting juvenile period (in rats) is correlated with the fact that ADHD patients are characterized by hyperactivity, which is most prominent during childhood. Moreover, in a rat model of ADHD where 6-hydroxydopamine (6-OHDA) was intracisternally administered during the neonatal period, it was the juvenile rats that showed an increase in spontaneous motor

* To whom correspondence should be addressed. Dr. Randeep Rakwal, HTRC, AIST, Tsukuba West, 16-1 Onogawa, Tsukuba 305-8569, Japan. E-mail, rakwal-68@aist.go.jp; fax, +81-29-861-8508.

† Human Stress Signal Research Center (HSS), National Institute of Advanced Industrial Science and Technology (AIST).

‡ Hokkaido University.

§ HSS, AIST Kansai Center.

10.1021/pr800025t CCC: $40.75

Published on Web 05/06/2008

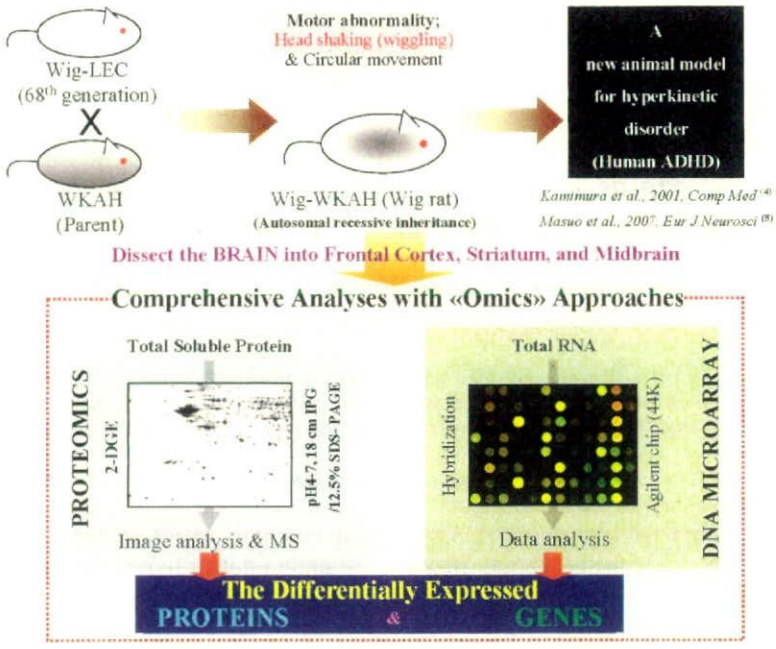

Figure 1. The Wig rat and a workflow representing the systematic omics approaches used for investigating the changes in protein and genes in the 3 dissected brain regions of Wig rat.

activity (SMA), which corresponds to preadolescence in humans.[5–7] Masuo and co-workers recently examined juvenile Wig rats, finding abnormalities in the SMA and development of DA neurons.[8] Moreover, when a cDNA macroarray (Atlas Rat 1.2, BD Biosciences Clontech) was used, changes in the expression of multiple genes, such as adenosine A2a receptor, macrophage migration inhibitory factor, and calbindin 2, were detected in 3 brain regions (frontal cortex, striatum, and midbrain) of these juvenile Wig rats over the control WKAH rats. These two studies preliminarily uncovered an aspect of Wig rat as an important animal model for ADHD, but further investigation is necessary to (1) uncover in greater detail the gene expressions at a global level using DNA microarray-based screening in these 3 regions, (2) look into the corresponding protein level changes, and (3) elucidate the mechanisms of the hyperactivity in Wig rat. Furthermore, it has been reported that the frontal cortex and ventral striatum, including the nucleus accumbens, may play crucial roles in ADHD.[1,9] We also separated the midbrain, since this region contains the substantia nigra and ventral tegmental area, regions rich in DA neurons.

To achieve this goal, we have selected two global "omics" approaches, namely, proteomics[10–12] and transcriptomics,[13–15] prominent and well-established technologies widely applied to address the biological questions in animals and other organisms. Our group has recently started focusing on gel-based (two-dimensional gel electrophoresis, 2-DGE) proteomics of the rat brain regions[16] with an aim to use this approach for a comprehensive investigation of stress-related protein profiling in the brain.[16] Moreover, our initial work in this direction has resulted in an improved protein extraction/solubilization protocol for brain proteomics.[16] This method involves the use of finely ground brain/brain regions in liquid nitrogen, before precipitating the total proteins with trichloroacetic acid (TCA)/acetone extraction buffer (TCAAEB) followed by solubilization of proteins in lysis buffer (LB). On the other hand, DNA microarray analysis is routinely employed for unraveling the genome-wide expression profiles and for screening of the genes of interest. The drawback is that this powerful genomic tool does not provide any direct information on protein levels and their state of modifications, mainly due to post-translation regulation, which results in a lack of correlation between mRNA and protein abundance.[17] As 2-DGE-based proteomics approach lacks wide coverage, it would be advantageous to employ a combination of proteomics and transcriptomics to any study where the identification of target molecular components (genes and proteins) is one of the goals (Figure 1).

Nevertheless, both these technologies are powerful screening methods for surveying the proteins and genes of interest in a particular sample, in our case, the Wig rat brain. In the present study, we have investigated the proteomes of precisely dissected frontal cortex, striatum and midbrain by 2-DGE in conjunction with peptide mass finger printing (PMF) methods (matrix-assisted laser desorption/ionization mass spectrometry, MALDI-TOF-MS), and tandem mass spectrometry by Q-TOF-MS/MS and nano electrospray ionization liquid chromatography–mass spectrometry (nESI-LC-MS/MS) for protein identifications. In parallel, DNA microarray analysis, along with reverse transcriptase-polymerase chain reaction (RT-PCR) experiments, was used to unravel the transcriptomes in these same brain regions.

2. Materials and Methods

2.1. Growth Conditions and Dissection of Brain. The experiments were carried out in accordance (Guidelines for the Care and Use of Laboratory Animals in the National Institute for Environmental Studies, Japan, and in the National Institute of Advanced Industrial Science and Technology, Japan) with the regional legal regulations. Male Wig and WKAH rats were housed in acrylic cage at 22 °C with tap water and laboratory chow *ad libitum*. The breeding rooms were illuminated from 07:00 to 19:00 h in 12 h cycles. The rats were decapitated at 4 weeks of age, whole brains were rapidly

removed, and whenever required, the frontal cortex, striatum, and midbrain were separated on ice.[7,18] For the midbrain, we made a frontal section between the anterior and posterior edges of the substantia nigra in order to investigate alterations in the region rich in dopaminergic neurons. On the other hand, the frontal cortex and striatum were dissected with the method of Glowinski and Iversen[19] with some modifications.[16,19] Each sample was immediately weighed, flash-frozen in liquid nitrogen, and stored at −80 °C until extraction of total crude protein.

2.2. Extraction of Total Protein. Extraction of total protein was performed using a two-step protein extraction protocol.[16,20] The three brain regions dissected from each rat were individually prepared for extraction of proteins. Briefly, frozen brain regions were separately placed in liquid nitrogen, and ground thoroughly to a very fine powder with a mortar and pestle. The tissue powder (ca. 50−100 mg) was transferred to sterile tubes containing cold TCAAEB (acetone containing 10% (w/v) TCA, and 0.07% mercaptoethanol), and the proteins were precipitated for 1 h at −20 °C, followed by centrifugation at 17 400*g* for 15 min at 4 °C. The supernatant was decanted, and the pellet was washed twice with chilled wash buffer (acetone containing 0.07% mercaptoethanol, 2 mM EDTA, and two EDTA-free proteinase inhibitor cocktail tablets (Roche Diagnostics GmbH, Mannheim, Germany) in a final volume of 100 mLbuffer), followed by removal of all the acetone. The pellet was subsequently solubilized in LB [7 M urea, 2 M thiourea, 4% (w/v) CHAPS, 18 mM Tris-HCl (pH 8.0), 14 mM Trizma base, two EDTA-free proteinase inhibitor cocktail tablets in a final volume of 100 mL buffer, and 0.2% (v/v) Triton X-100 (R), containing 50 mM dithiothreitol (DTT); hereafter called LB-TT], incubated for 20 min at 4 °C with occasional vortexing, and centrifuged at 17 400*g* for 15 min at 10 °C. In this experiment, a further purification/clean up of the solubilized protein samples was done by precipitating the supernatant at the last step with 4 vol of cold (−20 °C) acetone followed by resolubilization in LB-TT as above. The supernatant was pooled from each sample set and was then used for protein determination by a Coomassie Plus (PIERCE, Rockford, IL) protein assay kit at room temperature (RT), and stored in aliquots at −80 °C till analyzed by 2-DGE.

2.3. Two-Dimensional Gel Electrophoresis. 2-DGE was carried out using IPG strip gels (GE Healthcare Bio-Sciences AB, Uppsala, Sweden) on an IPGphor unit (GE Healthcare) followed by the second dimension using 12.5% polyacrylamide gels (PAGs) on a Nihon Eido (Tokyo, Japan) sodium dodecyl sulfate-PAG electrophoresis (SDS-PAGE) vertical electrophoresis unit. The volume carrying 125 μg of total soluble protein was mixed with LB-TT containing 0.5% (v/v) pH 4−7 IPG buffer to bring to a final volume of 350 μL. A trace of bromophenol blue (BPB) was added and the whole mixture was kept at RT for 5 min, vortexed, and centrifuged at 17 400*g* for 15 min at 10 °C followed by pipetting into a 18 cm strip holder tray. IPG strips (pH 4−7; 18 cm) were carefully placed onto the protein samples, covered with a lid, and placed into the IPGphor unit. The IPG strips were placed gel-face down onto the protein samples avoiding air bubbles and allowed to passively rehydrate with the protein samples for 1.5 h, followed by overlaying the IPG strips with 1000 μL of cover fluid, and this was directly linked to a five-step active rehydration and focusing protocol (18 cm strip) as described previously.[16] The whole procedure was carried out at 20 °C, and a total of 68 902 Vh was used for the 18 cm strip. Following IEF, the IPG strips were immediately used for the second dimension or stored at −20 °C.

The strip gels were incubated in equilibration buffer (50 mM Tris-HCl (pH 8.8), 6 M urea, 30% (v/v) glycerol, and 2% (w/v) SDS) containing 2% (w/v) DTT for 10 min (twice) with gentle agitation, followed by incubation in the same equilibration buffer supplemented with 2.5% (w/v) iodoacetamide twice at RT. Preceding the second-dimension separation, IPG strips were then rinsed with cathode running buffer [0.025 M Tris, 0.192 M glycine and 0.2% (w/v) SDS], placed onto polyacrylamide gels and overlaid with overlay agarose solution [60 mM Tris-HCl, pH 6.8, 60 mM SDS, 0.5% (w/v) agarose, and 0.01% (w/v) BPB]. The lower anode buffer contained 0.05 M diethanolamine and 0.05 M acetic acid. SDS-PAGE (4% T, 2.6% C stacking gels, pH 6.8, and 12.5% T, 2.6% C separating gels, pH 8.8) as the second dimension was carried out at constant current of 40 mA/per 18 cm gels for ca. 4.5 h. The % T is the total monomer concentration expressed in grams per 100 mL and % C is the percentage cross-linker. The stacking and separating gel buffer concentrations were 0.125 M Tris-HCl, pH 6.8, and 0.375 M Tris-HCl, pH 8.8, respectively. Molecular masses were determined by running standard protein markers (DualColor PrecisionPlus Protein Standard; Bio-Rad). For each sample, triplicate IPG strips and PAGs were processed for electrophoresis under the same conditions.

2.4. Protein Visualization and Spot Quantitation. To visualize the protein spots, the polyacrylamide gels were stained with silver nitrate (Plus One Silver Staining Kit Protein; GE Healthcare). Protein patterns in the gels were recorded as digitalized images using a digital scanner (CanoScan 8000F, resolution 300 dpi), and saved as TIFF files. The gels were quantitated in profile mode as instructed in the operating manual of the ImageMaster 2D Platinum software ver. 5.0 (GE Healthcare). To analyze differentially expressed spots, relative ratio of spot volume over the corresponding spot in control was calculated using the software. These results (spot differences) were also manually (visually) confirmed. Moreover, the silver nitrate stained spots were selected for comparative profiling only if they were confirmed in all three independent gel replications. Differentially expressed spots were defined as the ratio by more than 1.2-fold for increment or less than 0.8-fold for decrement in all three gel replications.[20] The differentially expressed spots were excised from the 2-D gels using a gel picker (One Touch Spot Picker, P2D1.5 and 3.0, The Gel Company, San Francisco, CA), and stored at −30 °C.

2.5. MALDI-TOF-MS and Q-TOF-MS/MS. Proteins were identified by PMF methods and tandem mass spectrometry.

2.5.1. MALDI-TOF-MS. In case of PMF, the excised gel spots were destained with 100 μL of destain solution [30 mM potassium ferricyanide (Sigma-Aldrich, St. Louis, MO), in 100 mM sodium thiosulfate (Merck, Darmstadt, Germany)], with shaking for 5 min. After the solution was removed, the gel spots were incubated with 200 mM ammonium bicarbonate (Sigma; and hereafter called AMBIC) for 20 min. The gel pieces were dried in a speed vacuum concentrator for 5 min and then rehydrated with 20 μL of 50 mM AMBIC containing 0.2 μg of modified trypsin (Promega, Madison, WI) for 45 min on ice. After removal of solution, 30 μL of 50 mM AMBIC was added and the digestion was performed overnight at 37 °C. The peptides were desalted and concentrated using C18 nanoscale (porus C18) column (homemade). For the analysis of MALDI-TOF MS by PMF method, the peptides were eluted by 0.8 μL of matrix solution [70% acetonitrile (Merck), 0.1% TFA (Merck), and 10 mg/mL α-cyano-4-hydroxycinamic acid (Sigma)]. The eluted peptides were spotted onto a stainless steel target plate.

Masses of peptides were determined using MALDI-TOF-MS (Model M@LDI-R; Micromass, Manchester, U.K.). Calibration was performed using internal mass of trypsin autodigestion product (m/z 2211.105).

2.5.2. Q-TOF-MS/MS. For analyses by MS/MS, 15 μL of the peptide solutions from the digestion supernatant (section 2.5.1) was diluted with 30 μL in 5% formic acid, loaded onto the column, and washed with 30 μL of 5% formic acid. Peptides were eluted with 2 μL methanol/H_2O/formic acid (50/49/1, v/v/v) directly into precoated borosilicate nanoelectrospray needles (EconoTip, New Objective). MS/MS of peptides generated by in-gel digestion was performed by nano-ESI on a Q-TOF2 MS (Micromass). The source temperature was 80 °C. A potential of 1 kV was applied to the precoated borosilicate nanoelectrospray needles in the ion source combined with a nitrogen backpressure of 0−5 psi to produce a stable flow rate (10−30 nL/min). The mass spectrometer was operated in an automatic data-dependent MS/MS to collect ion signals from the eluted peptides. In this mode, the most abundant peptide ion peak with doubly or triply charged ion in a full scan mass spectrum (m/z 400−1500) was selected as the precursor ion. Finally, an MS/MS spectrum was recorded to confirm the sequence of the precursor ion using collision-induced dissociation (CID) with a relative collision energy dependent on molecular weight. The cone voltage was 40 V. The quadrupole analyzer was used to select precursor ions for fragmentation in the hexapole collision cell. The collision gas was Ar at a pressure of $(6 \sim 7) \times 10^{-5}$ mbar and the collision energy was 20−30 V. Product ions were analyzed using an orthogonal TOF analyzer, fitted with a reflector, a microchannel plate detector and a time-to-digital converter. The data were processed using a MassLynx (Ver. 3.5) Windows NT PC system.

2.5.3. Protein Identification. Protein identification was performed by searching the National Center for Biotechnology Information (NCBI) nonredundant database using the MASCOT search engine (Matrix Science, Inc., London, U.K.; www.matrixscience.com), which uses a probability-based scoring system.[21] The following parameters were used for database searches with MALDI-TOF PMF data: monoisotopic mass, 50 ppm mass accuracy, trypsin as digesting enzyme with 1 missed cleavage allowed, carbamidomethylation of cysteine as a fixed modification, oxidation of methionine, N-terminal pyroglutamic acid from glutamic acid or glutamine as allowable variable modifications. For database searches with MS/MS spectra, the following parameters were used: average mass; 1.0 Da peptide and MS/MS mass tolerance; peptide charge of +1, +2, or +3; trypsin as digesting enzyme with 1 missed cleavage allowed; carbamidomethylation of cysteine as a fixed modification; oxidation of methionine as allowable variable modifications. Taxonomy was limited to mammalia for both MALDI and MS/MS ion searches. For MALDI-TOF-MS data to qualify as a positive identification, a protein's score had to equal or exceed the minimum significant score. Positive identification of proteins by MS/MS analysis required a minimum of two unique peptides, with at least one peptide having a significant ion score. The identified peptides are listed in Supplementary Table 1.

2.6. nESI-LC-MS/MS. Differentially expressed protein spots were digested with sequencing-grade modified trypsin according to a previous procedure[22] with minor modifications. Briefly, protein spots were washed twice with 100 mM AMBIC and then dehydrated with acetonitrile. The gel pieces were reduced with 10 mM DTT at 56 °C for 45 min and alkylated with 50 mM iodoacetamide for 45 min at RT in the dark in AMBIC solution. Gel pieces were washed with 20 mM AMBIC, dehydrated with acetonitrile, and air-dried. Gel pieces were subjected to in-gel trypsin digestion with 30 μL of 20 mM AMBIC containing 15 ng/μL sequence-grade modified trypsin (17 000 U/mg; Promega) at 37 °C for 18 h. The peptides were extracted from the gel pieces twice with 20 μL of 20 mM AMBIC and three times with 20 μL of 0.5% trifluoroacetic acid (TFA) in 50% acetonitrile. The peptides extracted in the five steps were combined together and concentrated to 20 μL by using a centrifugal concentrator (CC-105; TOMY, Tokyo, Japan). The peptides in 20 μL were used for mass spectral analysis on a LCQ Deca linear ion trap mass spectrometer (nESI-LC-MS/MS; Thermo Electron, Waltham, MA) through a nanoelectrospray ionization source. Briefly, online capillary LC included a monolithic reverse-phase trap column (0.2 mm × 5 cm, MonoCap for fast-flow, GL Science, Tokyo, Japan) and a fast-equilibrating C18 capillary column (monolith-type column; i.d., 0.1 mm; length, 50 mm; GL Science). Sample was loaded onto peptide traps for concentration and desalting prior to final separation by C18 column using a linear acetonitrile gradient ranging from 5% to 65% solvent B [H_2O/acetonitrile/formic acid, 10/90/0.1 (v/v)] in solvent A [H_2O/acetonitrile/formic acid, 98/2/0.1 (v/v)] for a duration of 40 min. The mass/charge (m/z) ratios of eluted peptides and fragmented ions from fused-silica Fortis Tip emitter (150 μM o.d., 20 μM i.d.; AMR, Inc., Tokyo, Japan) were analyzed in the data-dependent positive acquisition mode on LC-MS/MS. Dynamic exclusion used was repeat count (2), repeat duration (0.5 min), exclusion list size (25), and exclusion duration (3.0 min). Following each full scan (m/z 400−2000), a data-dependent triggered MS/MS scan for the most intense parent ion was acquired. The heated fused-silica Fortis Tip emitter was held at ion sprays of 1.8 kV and a flow rate of 300 nL/min.

Acquired LC-MS/MS data were submitted to a local MASCOT (version 2.1) server for querying all MS/MS ion search against NCBInr (Rat Protein Database, update 2006.09.09). The typical parameters used in the MASCOT MS/MS ion search were maximum of one trypsin miss cleavage, fixed modification of cysteine carbamidomethylation, variable modification of methionine oxidation, peptide mass tolerance of ±2 Da, threshold ($p < 0.05$), minimum ion counts (0), and fragment mass tolerance of ±0.8 Da. Criteria applied for unambiguous assignments of all proteins were a minimum of two nonredundant peptides with a score higher than 39. The identified peptides are listed in Supplementary Table 1.

2.7. 1-DGE, Subcellular Fractionation, and Western Analysis. Proteins were fractionated from tissue powder (ca. 50−100 mg) of the brain regions using the ProteoExtract Subcellular Proteome Extraction Kit (EMD Chemicals, Inc., Darmstadt, Germany) as per the instructions provided along with the kit. Soluble protein samples of each fraction were further purified using the 2-D Clean-Up Kit (GE Healthcare) and resolubilized in LB-TT. Proteins in the supernatant were quantified using Coomassie Plus protein assay kit, and stored in aliquots at −80 °C until analyzed. Prior to SDS-PAGE, 50 μL of each fractionated protein sample was mixed with 20 μL of SDS sample buffer [62 mM Tris (pH 6.8), 10% (v/v) glycerol, 2.5% (w/v) SDS, and 5% (v/v) 2-mercaptoethanol] and a drop of BPB. After incubation on the bench (ambient RT of 25 °C) for 10 min, the mixture was centrifuged, and a total of 5 μg of

Table 1. Primer Combinations Used for RT-PCR of Genes Encoding the Changed Proteins Identified by 2-DGE Analysis

		forward primer		reverse primer			
accession (gene)	spot number[a]	primer name	nucleotide sequence (5′−3′)	primer name	nucleotide sequence (5′−3′)	product size (bp)	number of cycles
NM_031603.1	6, 55, 77	RB091	CGATGGTGAAGAGCAGAATAAA	RB092	GGGACCAGTAAAATCCACAGAA	300	22
BC085120	8, 10, 45, 46, 47	RB103	CTTGCTGTACGAAACAGCACTC	RB104	GTTTTCATGCCACACAGATGTT	320	20
Z46882.1	13, 14	RB107	GCTCAGATTGACGACAACATTC	RB108	TCATGACTGTGTAGGGACTTGG	304	35
AF389425.1	15, 16	RB109	AAGATCATGCTGGAAGATGGTAA	RB110	AGACTAAATCCCGACTGATGGA	269	33
XM_215069.3	19	RB111	CCCAGGTTTATATCCTCAGCAA	RB112	TCAGCTCCATTTGATGTTCTTG	299	25
AB027144.1	21, 22	RB113	AGCAGATGACCAGCAAACTCAC	RB114	GGTCAGCACCAATTCTGTAGTG	295	35
NM_021774.1	26	RB119	TGAATAGGAAACCCGTTGTACC	RB120	GCTGGTGAGTCCTCTTCTTCTC	310	28
X54531.1	49	RB135	AGCCAGTGAGACTGAGGAGAAC	RB136	CTCCTTCAGTGCGTGGTACATA	307	30
XM_342542.2	50	RB137	AAAGATCCAGACTGCTTCAAGG	RB138	ACTGGTCTCACTGTGTGGAAGA	296	30
NM_022402.1	54	RB117	TGCAGCTGATAAAGACTGGAGA	RB118	CCAGTGGGAAGGTGTAGTCAGT	312	22
NM_013011.2	56, 57, 58	RB145	GCCCTCAACTTCTCTGTGTTCT	RB146	AGCATGGATGACAAATGGTCTA	294	20
X66974.1	61	RB147	AGAGTTCAATGCCATCTTCACA	RB148	GTTTCAAGAGAGTCAGGGCAGT	297	25
BC065582	62	RB149	CCATCGTCTATGAACTGGACAA	RB150	TGCCGGGGATAAAATACTAAAA	295	25
NM_017236.1	74	RB163	GGGAGTTCTCAGTTGTGCTAGG	RB164	GAATGCAATGCCCTTTATTTGT	307	22
XM_575249.1	75	RB089	TCCAGCATTTACTGACTCCAGA	RB090	TGGCTGGCTTATTTACAACAAA	316	30
BC088850.1	79	RB169	GACACGCTGAAGAAGCTGAATA	RB170	GTGGAGCTTGCATGTGAACTTA	295	25
BC098897.1	82	RB175	TCAGTTATCGCACTCGAGAAGA	RB176	CGCCCATCCATCTAATACTCTC	303	25
XM_574007.2	101	RB179	CTGAATTCCTGGACATCATCAA	RB180	CAAAGGGACAGCCAGTTCTACT	299	33

[a] Spot numbers correspond to the numbers indicated in Figures 1 and 2.

protein was loaded per sample/well. 1-DGE was carried out using 12.5% PAGs at constant current of 40 mA for ca. 3 h. The running buffer was composed of 0.025 M Tris, 0.192 M glycine, and 0.2% (w/v) SDS.

Electrotransfer of proteins on 1-D gel to a polyvinyldifluoride (PVDF) membrane (NT-31, 0.45 μM pore size; Nihon Eido) was carried out at 1 mA/cm^2 for 80 min using a semidry blotter (Nihon Eido) as described.[23] The anti-heat shock protein (HSP) 90 monoclonal antibody was commercially obtained from Abcam Ltd. (Cambridgeshire, U.K.). The ECL+plus Western Blotting Detection System protocol for blocking, primary and secondary antibody (anti-Rat IgG-H&L, Horseradish peroxidase linked whole antibody; from rabbit) incubation was followed exactly as described (GE Healthcare, Little Chalfont, Buckinghamshire, U.K.). Immunoassayed proteins were visualized on an X-ray film (X-OMAT AR, Kodak, Tokyo, Japan) using an enhanced chemiluminescence protocol according to the manufacturer's directions.

2.8. RT-PCR. Total RNA was isolated from ca. 50−100 mg of brain tissues using QIAGEN RNeasy Mini Kit (QIAGEN, MD). The quality of RNA is the single most important factor in determining the outcome of any transcriptomics analysis, and for this, the yield and RNA purity were determined spectrophotometrically (NanoDrop, Wilmington, DE) and visually confirmed using formaldehyde-agarose gel electrophoresis. Briefly, total RNA samples were DNase-treated with an RNase-free DNase (Stratagene, La Jolla, CA) prior to RT-PCR. First-strand cDNA was synthesized in a 50 μL reaction mixture with a StartaScript RT-PCR Kit (Stratagene) according to the protocol provided by the manufacturer, using 10 μg of total RNA isolated from frontal cortex, striatum and midbrain of Wig rat and control. The 50 μL reaction mixture (in 1× buffer recommended by the manufacturer of the polymerase) contained 1.0 μL of the first-strand cDNA from above, 200 mM dNTPs, 10 pmol of each primer set, and 0.5 U of Taq polymerase (TaKaRa Ex Taq Hot Start Version, TaKaRa Shuzo, Shiga, Japan). Specific primers were designed from the 3′-UTR regions (forward and reverse primer sequences are provided in Table 1) of each of the genes used in this study by comparison and alignment with all available related genes in the databases, NCBI. Thermal-cycling parameters were as follows: after an initial denaturation at 97 °C for 5 min, samples were subjected to a cycling regime of 20−35 cycles at 95 °C for 45 s, 55 °C for 45 s, and 72 °C for 1 min. At the end of the final cycle, an additional extension step was carried out for 10 min at 72 °C (TaKaRa PCR Thermal Cycle Dice, Model TP600, TaKaRa, Tokyo, Japan). After completion of the PCR, the total reaction mixture was mixed with 2.0 μL of 10× loading buffer and vortexed, 10 μL of the mixture was loaded into wells of a 1.5% agarose (Agarose ME, Iwai Chemicals, Tokyo, Japan) gel, and electrophoresis was performed for ca. 30 min at 100 V in 1× TAE buffer, using a Mupid-ex electrophoresis system (ADVANCE, Tokyo, Japan). The gels were stained (20 μL of 50 mg/mL Ethidium bromide in 100 mL 1× TAE buffer) for ca. 10 min, and the stained bands were visualized using an UV-transilluminator (ATTO, Tokyo, Japan).

2.9. Transcriptomics Analysis and Validatory RT-PCR. A rat 44K whole genome oligo DNA microarray chip (G4131A, Agilent Technologies, Palo Alto, CA) was used for the microarray experiment. Total RNA from each (150 ng) of the 3 brain regions (frontal cortex, striatum and midbrain) was pooled together into one master total RNA mix (450 ng), and labeled with Cy-3 or Cy-5 using an Agilent Low RNA Input Fluorescent Linear Amplification Kit (Agilent). Fluorescently labeled targets of control and Wig samples were hybridized to the same microarray slide with 60-mer probes. A flip labeling (dye-swap or reverse labeling with Cy3 and Cy5 dyes) procedure was followed to nullify the dye bias associated with unequal incorporation of the two Cy dyes into cDNA.[24−26] In our experience, the use of a dye-swap approach[27] provides a very stringent selection condition for changed genes rather than simply doing 2 or 3 replicates, which overlook the dye bias. The design of the microarray experiment is presented in Table 2. Hybridization and wash processes were performed according to the manufacturer's instructions, and hybridized microarrays were scanned using an Agilent Microarray scanner G2565BA.

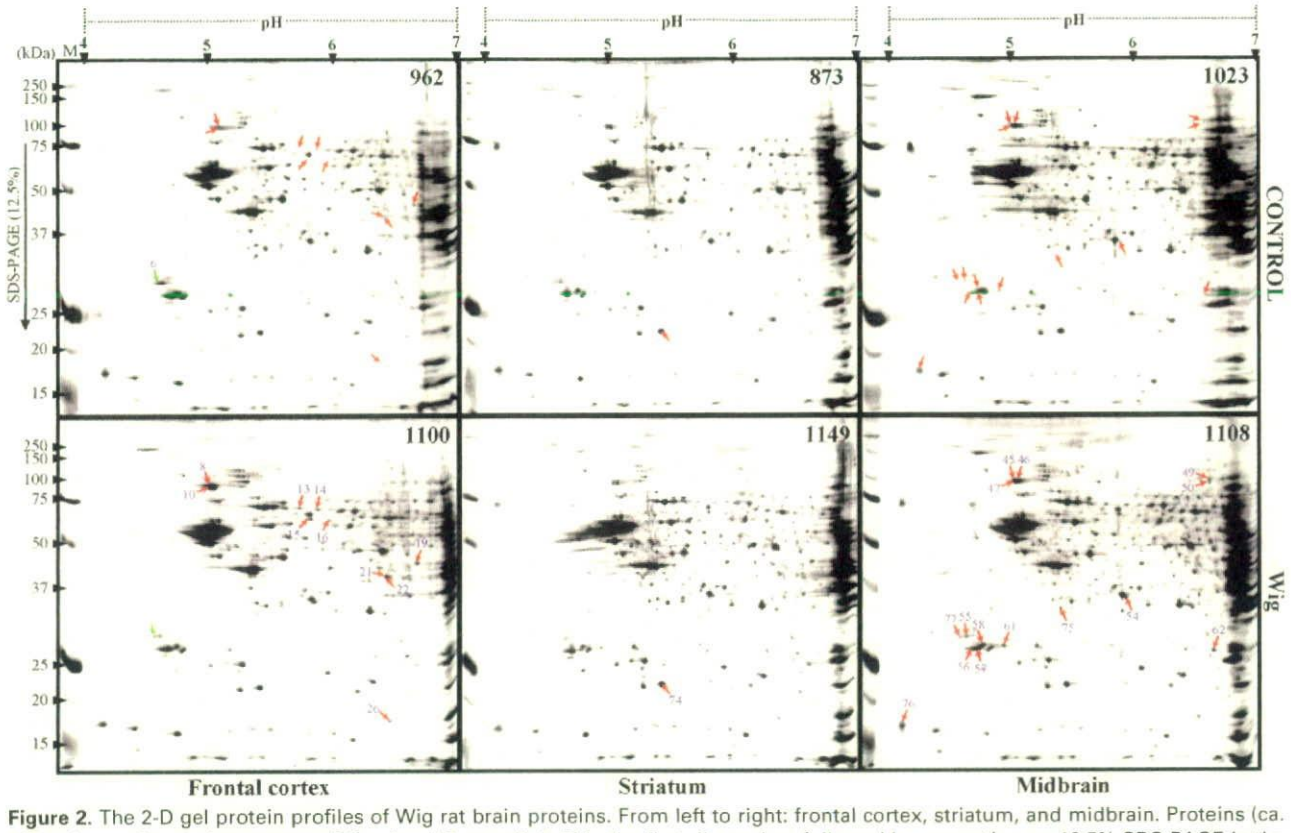

Figure 2. The 2-D gel protein profiles of Wig rat brain proteins. From left to right: frontal cortex, striatum, and midbrain. Proteins (ca. 125 μg) were focused on precast IPG strips (18 cm, pH 4−7) in the first dimension; followed by separation on 12.5% SDS-PAGE in the second dimension. The proteins were stained with silver nitrate, and image analysis was performed using the ImageMaster software. Isoelectric points (p*I*) and molecular mass standards (M, Precision Plus Protein Standards, Bio-Rad) are indicated on the top and the left-hand side, respectively. The numbers of detected spots in each gel by the software are given at the top right-hand corners. Differentially expressed protein spots in each of the three brain regions as compared with respective controls are marked by arrows and numbers, and were taken for MS (MALDI-TOF-MS and Q-TOF-MS/MS) analyses. Red arrows show induced spots and green arrows show suppressed spots, respectively, over the controls.

Table 2. Details of Microarray Experiment

			labeling	
replicate[a]	sample	microarray slide no.	Cy3	Cy5
Pooled Biological Replicates (×3)	BRAIN[b]	MA 1	Control	Wig
		MA 2	Wig	Control
		RT-PCR validation[c]		

[a] Total RNA isolated from individual rat brain regions was used for cDNA synthesis. [b] Pooled three regions: frontal cortex, striatum, and midbrain. [c] For RT-PCR validation, total RNA from each region was analyzed separately over the control.

For detection of significant differentially expressed genes between control and Wig samples, each slide image was processed by Agilent Feature Extraction ver.8.1.1.1. This software measured Cy3 and Cy5 signal intensities of whole probes. Dye-bias tends to be a signal intensity-dependent; therefore, this software selected a probe set by rank consistency filter for dye-normalization, and the normalization was done by LOWESS (locally weighted linear regression) and it calculated log ratio of dye-normalized Cy3- and Cy5-signal, and final error of log ratio and significant value (*P*-value) based on propagate error model and universal error model. In this analysis, the threshold of significant differentially expressed genes determined p-value < 0.01 for the confidence that the feature is not differentially expressed. In addition, erroneous data generated due to artifacts were eliminated before data analysis. Confirmatory RT-PCR was performed (see section 2.8) using 3′-UTR specific gene primers, which are listed in Table 3.

3. Results and Discussion

3.1. 2-DGE and MS Identify 19 Nonredundant Proteins. To investigate the alterations of protein profiles in the frontal cortex, striatum and midbrain of Wig rats over control WKAH rats, 2-DGE analysis of total soluble proteins from pooled three replicates was performed using 18 cm IPG strip format and 12.5% homogeneous SDS-PAGE. The representative 2-D gels stained with silver nitrate are shown in Figures 2 and 3. On 2-D gels of the three regions from Wig rats and controls, ca. 1000 spots in pH 4−7 range and 500 spots in pH 6−9 range were counted using the 2D ImageMaster software. To assess changes in protein profiles, relative ratio of spot volume was calculated using the software and changed (increased or decreased in Wig rat over control) spots were selected as mentioned in Materials and Methods. In Figure 4, average ratio of the selected spots in 3 independent gel replications is shown. In the frontal cortex, 11 spots (nos. 6, 8, 10, 13−16, 19, 21, 22, and 26) in pH 4−7 range and two spots (nos. 79 and 82) in pH 6−9 range were differentially expressed over control. In the striatum, one spot (no. 74) in pH 4−7 range and no spots in

Table 3. Primer combinations Used for Validatory RT-PCR of Genes Differential Expressed during Microarray Experiment

	forward primer		reverse primer		
accession (gene)	primer name	nucleotide sequence (5′−3′)	primer name	nucleotide sequence (5′−3′)	product size (bp)
XM_216315	RB319	GGCTGTGACATCTATCCCATCT	RB320	GTTAACTTTGCGGACATCTTCC	295
NM_031703	RB321	GATCAGTTCATAGGCACAGCAG	RB322	GTACACGAAGACACCACCAATG	297
NM_001014089	RB323	CCTGGCTAGGTTGTTCCCTAAT	RB324	GATACCTGAATGGCACTTCCTC	299
WIG 2007-1	*RB325*	*under patent application process*	*RB326*	*under patent application process*	*302*
XR_008769	RB331	AGTCGCGGATCCTGAAAGTAT	RB332	TTCATGATGATAGCCTCCTCCT	315
XM_001067936	RB333	GCCAAGTCCATAAAACAAAGGA	RB334	GGGCCTGTAGTAAAAATCCAGA	303
WIG 2007-2	*RB301*	*under patent application process*	*RB302*	*under patent application process*	*303*
EF125690	RB303	CTGTTTCCACCACACATTCCTA	RB304	ATCAATGTCAGTTACCGTGCTG	303
NM_001013210.1	RB305	TAGAGGACTACTGGGCTGCTCT	RB306	GGCCAAAGCTGTTAAGGAATAA	302
XM_001062086	RB307	CAGAAAACCCAAAAGGAAGATG	RB308	AGCCTTTGCTTTTTCAGTCAAC	310
NM_001009713	RB309	TTTTACGGCTACATCGTCACAC	RB310	CCGGAAAGAGGAAGTGAGATTA	308
XM_224672	RB311	ACATCAGCCAACACCTAATCCT	RB312	CTGTTTTCACAGGACAAACTGG	302
XM_001080810	RB313	AAAATCCTCTGGCCTCTCCTAC	RB314	ATCTAGGAGCATGAAAGCCTTG	301
NM_001000282	RB315	AGCCTTTCCTGCTCTAACATTG	RB316	TTCAGCATGGGAATCACAATAC	302
NM_001005888	RB317	AAATCTTCAGCTGACTGCCTTC	RB318	TGACATCTTTGCATTCCAGACT	301

pH 6−9 range were differentially expressed over control. In the midbrain, 15 spots (nos. 45−47, 49, 50, 54−58, 61, 62, and 75−77) in pH 4−7 range and one spot (no. 101) in pH 6−9 range were differentially expressed over control. A total of 30 protein spots were analyzed by MALDI-TOF/Q-TOF MS (pH 4−7 range spots) and nESI-LC-MS/MS (spots in the pH range 6−9). From these, 19 nonredundant proteins were identified (Table 4).

3.2. RT-PCR Analysis of Corresponding Gene Expression. We also investigated whether these proteins are regulated at the mRNA level. The 3′-UTR specific primers of corresponding gene (cDNA) sequences were designed (Table 1) and used those for checking the transcript levels using RT-PCR (Figure 5). Corresponding protein spot numbers are given on the left-hand side of the individual gel images, respectively. RT-PCR results reveal the corresponding mRNA levels in the frontal cortex, striatum, and midbrain of 4-week-old Wig rat. For spots 6, 55, and 77; 13 and 14; 15 and 16; 19, 26, 49, 82, and 101, the alteration of mRNA levels was in parallel with that of protein spot levels in the brain region from which the protein spot was identified. For spot 101, alteration of mRNA level was in parallel with that of protein spot level in all the 3 brain regions. However, in many

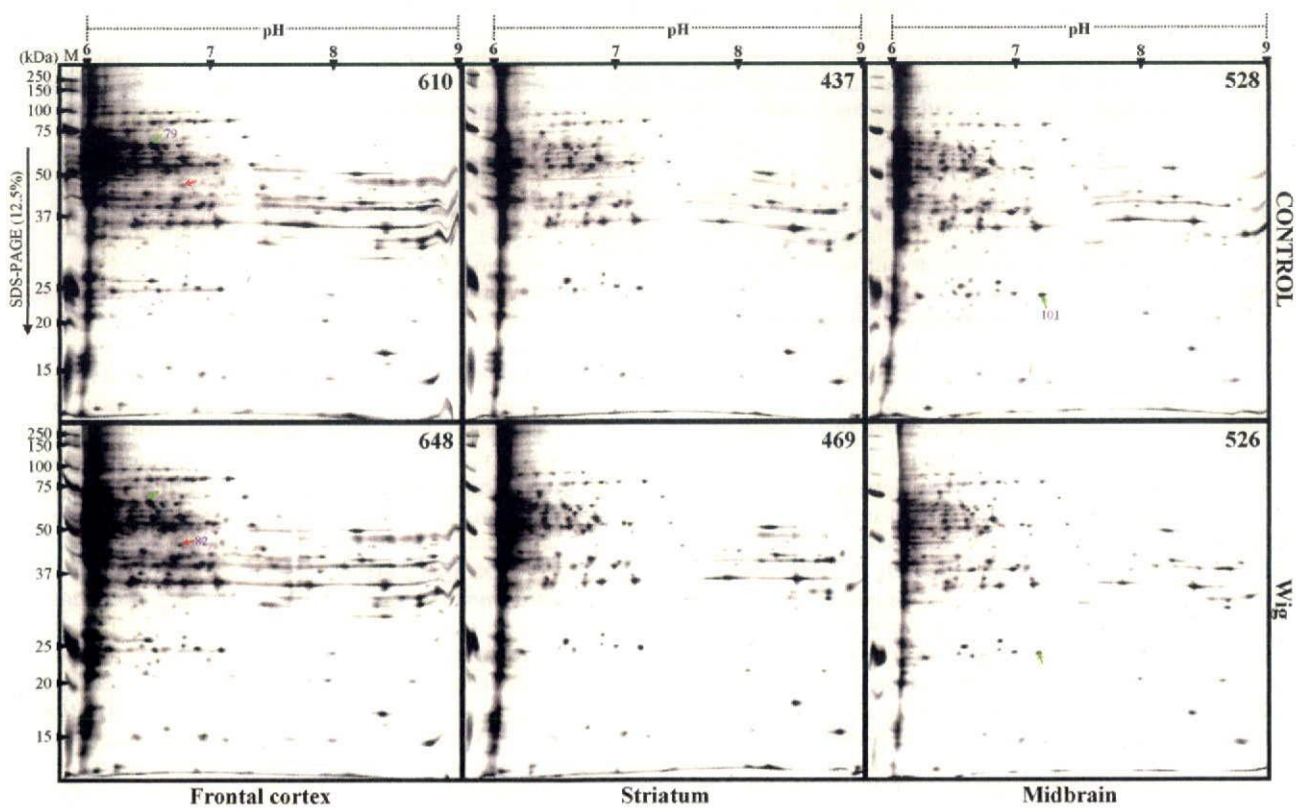

Figure 3. Silver nitrate stained 2-D gel basic protein profiles of frontal cortex, striatum, and midbrain. For separating proteins in the basic regions, pH 6−9 IPG strips (18 cm) was used. 2-DGE, image analysis, and spot markings are the same as in Figure 2.

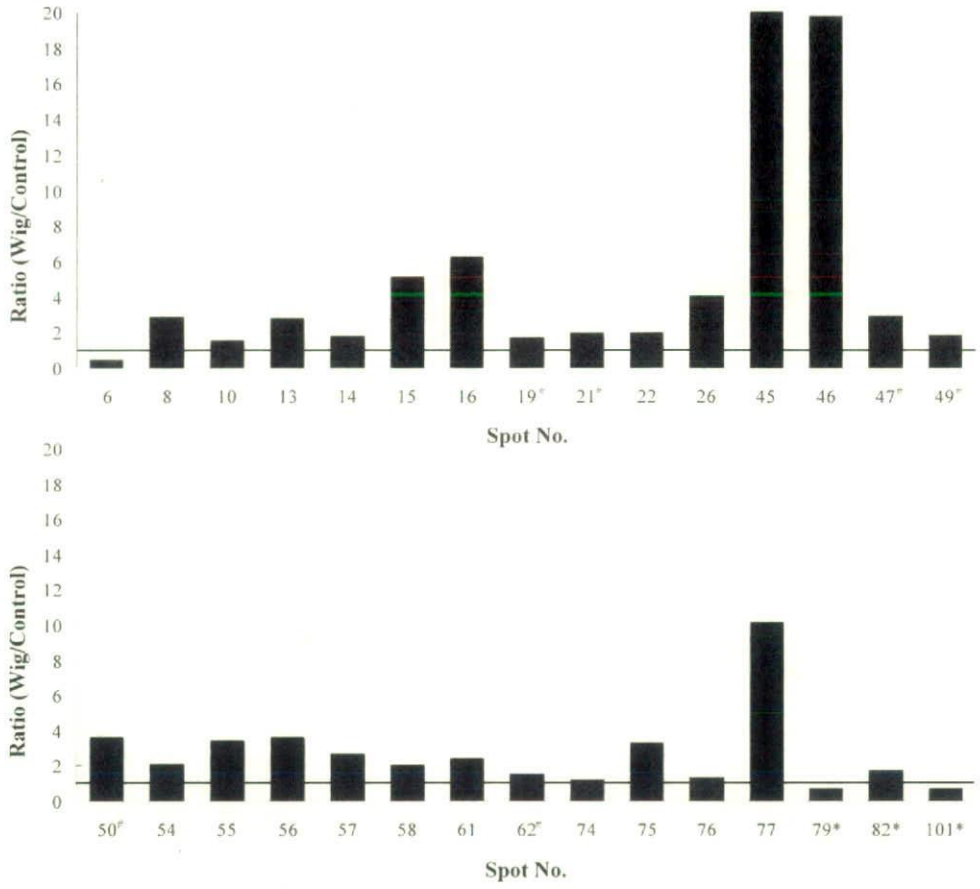

Figure 4. Graphical presentation of the differentially expressed protein spot volumes on 2-D gels of Wig rat frontal cortex, striatum, and midbrain. The corresponding spot numbers are the same as marked in Figures 2 and 3. The ratio (protein spots in Wig over control) of the differentially expressed spot volume was calculated using ImageMaster software. The volume of the corresponding spots in three gel replications altered more than 1.2-fold or less than 0.8-fold. Asterisks (*) indicate the protein spots marked in Figure 3. Sharps (#) indicate spots which were detected in just two gel replications of three gel replications. Horizontal line indicates 1.0-fold.

cases, there was no correlation between mRNA levels and protein spot levels, suggesting possibilities of the time-lag between transcription and translation and/or the occurrence of post-translational modification.

3.3. Functional Categorization and Subcellular Localization of Identified Proteins. The identified proteins were classified into seven functional categories (Figure 6A), namely, signal transduction (26.3%), energy metabolism (26.3%), cellular transport (15.8%), protein with binding function (10.5%), protein synthesis (10.5%), cell division/cytoskeleton (5.3%), and protein fate (5.3%). The functional categories were determined using NCBI database or Rat Genome Database (RGD, http://rgd.mcw.edu/). Use of a subcellular localization tool (PSORT II, http://psort.nibb.ac.jp/) revealed that 15 (78.9%) out of 19 proteins were cytoplasmic in nature, whereas three proteins were localized in the nucleus and one protein was extracellular (Figure 6B). In the following subsections, we will discuss the identified proteins based on their functional categories.

3.3.1. Signal Transduction. In the signal transduction category, 5 proteins showed changed expressions. The 14-3-3 proteins (spots 6, 55, and 77; epsilon isoform, spots 56−58; zeta isoform) have 7 isoforms and are mainly localized to the synapses and neuronal cytoplasm.[28] The 14-3-3 isoforms interact with phosphoserine motifs on many proteins as kinases, phosphatases, apoptosis-related proteins, and so forth.[29] Several reports have hinted at a possible relevance of 14-3-3 protein isoforms in neurological diseases.[28−30] Two reports have shown that the 14-3-3 zeta isoform is associated with tau protein, which is the main component of neurofibrillary tangles (NFTs), and an effector of tau phosphorylation on NFTs of Alzheimer's disease (AD).[31] It has also been reported that expression changes of the 14-3-3 epsilon protein might reflect impaired signaling and apoptosis in the brain regions of AD patients.[29] Our results reveal the induction of epsilon and zeta isoforms of 14-3-3 proteins in midbrain of Wig rats but a reduction in the epsilon isoform in the frontal cortex. It is possible that these derangements may be the cause of impaired signal transduction in the brain regions.

Dihydropyrimidase-related protein (DRP) 2 (spots 13 and 14) and collapsin response mediator protein (CRMP) 4 (spots 15 and 16) are members of cytosolic phosphoproteins that are involved in the signal transduction of semaphorin 3A leading to growth cone collapse. The activity and binding of DRP2, also known as CRMP2, are regulated via phosphorylation by glycogen synthase kinase 3 beta (GSK3b).[32] CRMP2 mediates the intracellular response to collapsin 1/semaphorin 3A, a repulsive extracellular guidance for axonal outgrowth, and is also involved in microtubule assembly.[33] Several reports have shown

Table 4. List of Identified Brain Proteins by Tandem Mass Spectrometry[a]

spot no	brain regions	MW (kDa)/p*I* observed	protein name	MW (da)/ p*I* theoritical	method	accession	score	sequence coverage	subcellular localization
			Signal Transduction						
6		29/4.5					89	27%	
55	FC and MB	28/4.6	**Chain A, 14-3-3 Protein Epsilon**	26912/4.92	MALDI-TOF	2BR9_A (NP_113791)	99	29%	Cytoplasm
77		27/4.5					129	35%	
13	FC	64/5.7	**Dihydropyrimidinase related protein-2 (DRP-2)**	62622/5.95	MALDI-TOF	XP_858120 (AAB07042)	147	31%	Cytoplasm
14		64/5.8							
15	FC	60/5.8	Collapsin response mediator protein 4 (CRMP4)	62327/6.04	MALDI-TOF	AAK64497	205	31%	Cytoplasm
16		59/5.9							
56		26/4.6							
57	MB	26/4.7	**14-3-3 Protein Zeta**	27879/4.72	MALDI-TOF	BAA11751 (NP_037143)	112	42%	Nuclear
58		27/4.7							
74	ST	19/5.4	**Phosphatidylethanolamine binding protein**	20902/5.48	MALDI-TOF	NP_058932	138	63%	Cytoplasm
			Energy Metabolism						
26	FC	17/6.4	Fragile histidine triad protein (Fhit)	17394/6.16	MALDI-TOF	AAC23967 (NP_068542)	77	62%	Cytoplasm
50	MB	92/6.6	**Brain glycogen phosphorylase**	97361/6.31	MALDI-TOF	XP_342543	277	32%	Cytoplasm
62	MB	26/6.6	**Phosphoglycerate mutase 1 (PGM1)**	28900/6.67	MALDI-TOF	AAH53356 (NP_445742)	131	47%	Cytoplasm
101	MB	25/7.1	**Triosephosphate isomerase (Tpi) 1 protein**	27214/7.07	ESI-MS/MS	AAH61781	215	50%	Cytoplasm
82	FC	48/6.8	Pyruvate dehydrogenase E1 alpha 1	43872/8.35	ESI-MS/MS	AAH98897	143	25%	Cytoplasm, Mitochondria
			Cellular Transport						
49	MB	98/6.6	**D100 (Dynamin 1)**	96209/6.32	MALDI-TOF	CAA38397	127	17%	Nuclear
75	MB	34/5.4	N-ethylmaleimide sensitive fusion protein attachment protein (SNAP)-beta	33850/5.32	MALDI-TOF	XP_534322 (XP_575249)	287	76%	Cytoplasm
79	FC	64/6.5	Syntaxin binding protein 1	67925/6.49	ESI-MS/MS	BAA32486 (AAH88850)	163	16%	Nuclear
			Protein with Binding Function						
61	MB	27/4.9	Calbindin 2 (Calretinin)	31467/4.94	MALDI-TOF	AAH17646 (CAA47385)	110	32%	Cytoplasm
76	MB	17/4.0	Solution structure of calcium-calmodulin N-terminal domain	8483/3.90	Q-TOF	1J7O_A (NP_114175)	38	17%	Cytoplasm
			Protein Synthesis						
19	FC	45/6.7	Tu translation elongation factor (EF-Tu)	56609/8.50	MALDI-TOF	XP_215069	149	29%	Extracellular, including cell wall
54	MB	37/5.9	Acidic ribosomal phosphoprotein PO	32527/5.28	MALDI-TOF	AAB65436 (NP_071797)	128	38%	Cytoplasm
			Cell Division/Cytoskeleton						
21	FC	42/6.4	**CDCrel-1AI**	42487/6.21	MALDI-TOF	BAB87114	194	40%	Cytoplasm
22		41/6.4							
			Cell Rescue						
8		86/5.0							
10		82/5.0					145	24%	
45	FC and MB	98/5.0	**Heat shock protein HSP 90-alpha**	83445/5.00	MALDI-TOF	Q9GKX7 (NP_786937)			Cytoplasm
46		98/5.0					174	25%	
47		94/5.0							

[a] Identified proteins were classified into functional categories. The altered proteins (>1.2-fold for increment or <0.8-fold for decrement) in the frontal cortex, striatum, and midbrain of Wig rats were identified using MALDI-TOF, Q-TOF, or LC-ESI-MS/MS. Differentially expressed spots in different brain regions are abbreviated as FC, frontal cortex; MB, midbrain; and ST, striatum. Bold letters indicate proteins reported to be involved in neurodegenerative diseases (e.g. Alzheimer's and Parkinson's disease, Schizophrenia) and mental disorders. Accession numbers in parentheses indicate *Rattus norvegicus* protein accessions.

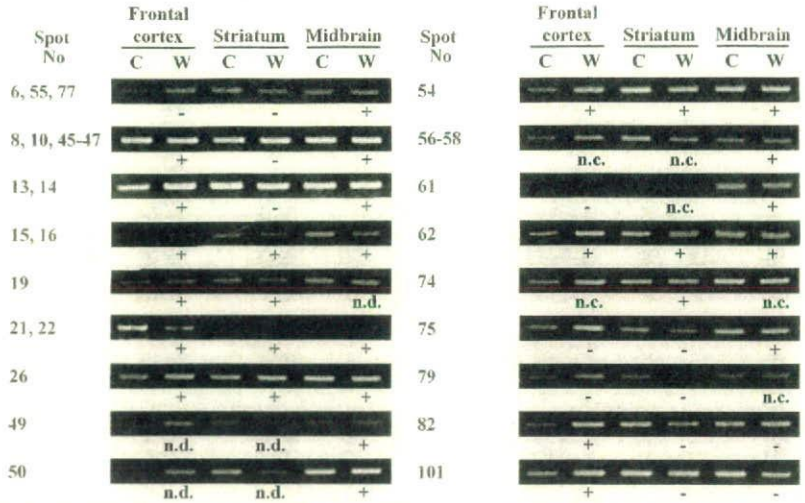

Figure 5. RT-PCR analysis of the genes encoding the differentially expressed proteins identified by 2-DGE. Protein spot numbers (the same as in Table 3) are given on the left-hand side of the gel image in parentheses. Marks and words given under gel images indicate expression changes of corresponding protein spots over controls on 2-D gel images of each brain regions. Plus (+) mean induced spots, minus (-) mean suppressed spots, and n.d., not detected; n.c., not changed; C, control; and W, Wig rat.

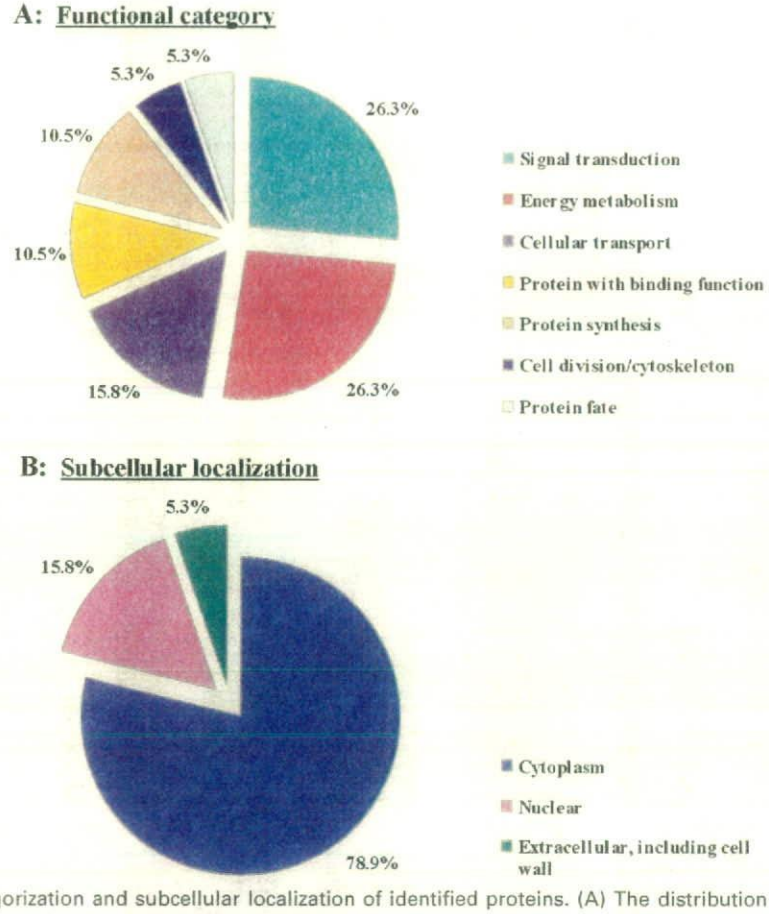

Figure 6. Functional categorization and subcellular localization of identified proteins. (A) The distribution of nonredundant proteins identified by MS analyses into functional categories determined using NCBI or Rat Genome Database; (B) the same (in above) protein distribution according to their subcellular localization determined using NCBI or Web tool PSORT II.

that the protein level of DRP2 was induced in anterior cingulated cortex of patients with schizophrenia (SCZ) and major depressive disorder (MDD).[34,35] CRMP2 and CRMP4 are also co-localized with F-actin of growth cone during discrete periods of neuronal development.[36,37] A recent report suggests that overexpression of CRMP4 inhibit cell migration due to its specific regulatory role toward the actin cytoskeleton.[36] The CRMP4 and DRP2 proteins were found to be increased in the frontal cortex, speculating that induction of those proteins may cause the abnormality of axon guidance. Since we previously